1964

Circular polarization measurements of gamma rays following the beta decay of Sb124 and Cs134

Kenneth Glenn Tirsell
Iowa State University

CIRCULAR POLARIZATION MEASUREMENTS OF GAMMA RAYS FOLLOWING THE BETA DECAY OF Sb^{124} AND Cs^{134}

by

Kenneth Glenn Tirsell

A Dissertation Submitted to the
Graduate Faculty in Partial Fulfillment of
The Requirements for the Degree of
DOCTOR OF PHILOSOPHY

Major Subject: Physics

Approved:

Signature was redacted for privacy.

In Charge of Major Work

Signature was redacted for privacy.

Head of Major Department

Signature was redacted for privacy.

Dean of Graduate College

Iowa State University
Of Science and Technology
Ames, Iowa

1964

TABLE OF CONTENTS

		Page
I.	INTRODUCTION	1
	A. Review of Beta Decay Theory	1
	B. Experiments Concerning Parity Nonconservation in Nuclear Beta Decay	9
	C. Previous Beta-Gamma Circular Polarization Measurements	13
	D. Motivation for the Experiment	15
II.	EXPERIMENTAL INVESTIGATION	17
	A. Selection of the Method	17
	B. Description of the Measurement	18
	C. Description of the Apparatus	20
	D. Performance Tests	28
	E. Experimental Procedure	34
III.	ANALYSIS OF DATA	50
	A. The Determination of Asymmetry Parameters	50
	B. The Calculation of the Response of the Circular Polarization Analyzer	57
IV.	EXPERIMENTAL RESULTS AND DISCUSSION	69
	A. Asymmetry Parameters	69
	B. Matrix Element Ratios	74
	C. Discussion	81
V.	SUMMARY	89
VI.	LITERATURE CITED	90
VII.	ACKNOWLEDGMENTS	95

I. INTRODUCTION

As a consequence of the nonconservation of parity* in weak interactions (1,2,3) the gamma radiation following nuclear beta decay is, in general, circularly polarized (4,5). From measurements of the degree of circular polarization information can be gained concerning the relative magnitudes of nuclear matrix elements involved in certain beta transitions. In this investigation circular polarization measurements of gamma rays following the beta decay of Sb^{124} and Cs^{134} have been made and nuclear matrix element ratios have been obtained. These measurements will be described following a brief outline of beta decay theory and, by way of introduction, a discussion of experiments concerned with parity nonconservation in beta decay.

A. Review of Beta Decay Theory

Several reviews of the theory of beta decay have been given in the literature (6,7,8,9). In this section a brief outline of the current status of the theory will be presented.

Nuclear beta decay of radioactive substances is a process in which the parent nucleus decays to a daughter nucleus with the simultaneous emission of an electron (beta ray) and an antineutrino. Positron emission is an analogous process in which a positive electron is emitted accompanied by a neutrino. The neutrino is a neutral particle with spin $\frac{1}{2}$ and apparently vanishing rest mass. The existence of such a particle was

---

*Conservation of parity requires that the results of an experiment on a system be indistinguishable from results obtained from a system which is its mirror image.

postulated to conserve energy and angular momentum in the decay.

Nuclear beta decay is treated in terms of a field theory in which the nucleons are the source of the field and the light particles referred to as leptons (electron and antineutrino) together make up the field. The leptons must be treated relativistically. Thus the theory resembles that for the absorption and emission of electromagnetic radiation. To describe the interaction a perturbation term was developed to be added to the free particle Hamiltonian for the nucleons and leptons. This beta-decay interaction energy density has the form (10)

$$H = g \sum_x \left(\psi_f^* O_x \psi_i \right) \left[\psi_e^* O_x \left(C_x + C_x' \gamma_5 \right) \psi_{\bar{\nu}} \right] + \text{Hermitian Conjugate},$$

where ψ_i and ψ_f are 4 component spinor wave functions representing the final and initial nuclear states, ψ_e and $\psi_{\bar{\nu}}$ represent electron and antineutrino ($\bar{\nu}$) states, g is a constant determining the strength of the interaction, and O_x is an operator corresponding to one of the five possible relativistically invariant forms: O_S, a scalar; O_V, a polar 4-vector; O_T, an antisymmetric 4-tensor; O_A, an axial 4-vector; and O_P, a pseudoscalar. The expression for H is an arbitrary linear combination of these forms. Each form is introduced by a coupling coefficient C_x. The old theory is modified by the addition of the couplings $C_x' \gamma_5$ to account for nonconservation of parity.

From first-order perturbation theory, the probability per unit time for the beta transition from an initial nuclear state ψ_i to a final state ψ_f is given by

$$N(W) = \frac{2\pi}{\hbar} \left| \left(\psi_f^* \left| H \right| \psi_i \right) \right|^2 \frac{\partial \rho}{\partial W} , \qquad (1)$$

where $\frac{\partial \rho}{\partial W}$ is the density of final states per unit of total electron energy W. Here the matrix elements are summed over all nucleons and integrated over the nuclear volume. A sum over all nonobserved quantities such as spin directions of leptons is also implied.

In a first approximation the Coulomb field acting on the electron is neglected. Both leptons are represented by plane waves, and a multipole expansion is made (10). The terms of the expansion correspond to increasing orders of orbital angular momentum ℓ carried off in the decay. The general matrix element corresponding to H assumes the form

$$\sum_{\ell} \left(\psi_f^* \left| O_{j\ell} \right| \psi_i \right) \left(P_\ell \, R \right)^\ell ,$$

where the operator $O_{j\ell}$ is related to the quantum numbers j and ℓ associated respectively with the total angular momentum and the orbital angular momentum carried off in the decay. P_ℓ is a Legendre polynomial and R is the nuclear radius. Since $(P_\ell \, R) \ll 1$, successive terms in the expansion decrease rapidly.

The nuclear matrix elements $\left(\psi_f^* \left| O_{j\ell} \right| \psi_i \right)$ have selection rules $j_f = j_i, \; j_i \pm 1, \ldots . j_i \pm j$, and $\Delta \pi = (-1)^\ell$, where j_i (j_f) is the initial (final) nuclear spin. Since $j = \ell \, , \ell \pm 1$, the allowed transitions corresponding to the largest term ($\ell = 0$) have selection rules $j = 0, 1$ and $\Delta \pi = +1$ (no parity change). The first-forbidden transitions correspond to $\ell = 1$ with $j = 0,1,2$ and $\Delta \pi = -1$. In general terms of order of forbiddenness ℓ in the expansion become important when selection rules in-

hibit the nuclear matrix elements of the preceeding terms.

Allowed transitions involving the emission of leptons in a singlet state ($j = 0$) with no orbital angular momentum carried off ($\ell = 0$) are designated as Fermi type, whereas emission in a triplet state ($j = 1$) is referred to as Gamow-Teller type. Gamow-Teller (G-T) transitions are not permitted in case $j_i = j_f = 0$ even though $j_i - j_f = 0$; therefore, such transitions are pure Fermi. Transitions involving $j_i - j_f = \pm 1$ are pure G-T. The allowed cases with $j_i = j_f \neq 0$ are mixed. Pseudoscalar transitions have $j_i - j_f = 0$ but also have $\Delta \pi = (-1)$ and are therefore first-forbidden. Effects due to pseudoscalar coupling and to the small nuclear velocity may be neglected in the allowed case. The assumption that Fermi coupling is mainly vector and G-T coupling is mainly axial-vector will be discussed later.

With these assumptions the energy spectrum $N(W)$ obtained from the transition probability in Equation 1 has the form

$$N(W)\, dW = \text{Const}\ F(Z,W)\ pW\ (W_o - W)^2\ \xi\ \left(1 - \frac{b}{W}\right) dW$$

The energy dependent factor $pW(W_o - W)^2$ comes from the density of final states $\frac{\partial \rho}{\partial W}$. Here W, the total electron energy, and W_o, the maximum total electron energy, are both in mc^2 units*. The energy independent factor ξ comes from the square of the transition matrix element given by

$$\left| \left(\psi_f^* \quad | H | \quad \psi_i \right) \right|^2 = F(Z,W)\ \xi.$$

---

*p, the electron momentum, is given by $p = (W^2 - 1)^{\frac{1}{2}}$.

The factor ξ depends only on the reduced matrix elements and beta decay coupling constants and is defined by

$$\xi = (|C_V|^2 + |C_V'|^2) |M_F|^2 + (|C_A|^2 + |C_A|^2) |M_{GT}|^2 ,$$

where $M_F = (\psi_f^* | O_V | \psi_i)$ is the Fermi matrix element and $M_{GT} = (\psi_f^* | O_A | \psi_i)$ is the Gamow-Teller matrix element. The Fermi function $F(Z,W)$ is a measure of the nuclear Coulomb effects on the electron wave function in the nucleus. Complete tabulations of the modified Fermi function, $G(Z,W) = Fp/W$, have been made (11). Note that if the end point energy W_o is known, the spectral shape of an allowed transition can be computed from these tables using

$$N(W) \propto G(Z,W) \; W^2 \; (W_o - W)^2 . \qquad (2)$$

It was here assumed that $b = 0$, since the Fierz constant b is presently thought to be negligible (12,13,14,15).

From Equation 2 we have

$$\left[\frac{N(W)}{G(Z,W) \; W^2} \right]^{\frac{1}{2}} = K' (W_o - W) ,$$

where the constant K' is independent of energy. A plot of the left hand side of this equation should give a straight line with intersection at $W = W_o$. Known as a Kurie (or Fermi) plot, this may be used to determine end point energies from observed spectra. Furthermore, deviations from linearity of known allowed decays are an indication of instrumental difficulties or the presence of branching in the decay.

The decay constant associated with the beta transition is obtained from

$$\lambda = \int_{1}^{W_o} N(W)\ dW = \text{Const}\ \xi\ f(Z,W_o),$$

where

$$f(Z,W_o) = \int_{1}^{W_o} pW(W_o - W)^2\ F(Z,W)\ dW.$$

The rate of decay of transitions with different W_o can be compared using the quantity $ft = \frac{f\text{Ln}2}{\lambda}$, where t is the half life. Thus, ft is called the comparative lifetime and is related to the nuclear matrix elements for allowed transitions by

$$ft = \frac{\text{Ln}2}{\text{Const}\ \xi} = \frac{K}{M_F^2 + R\ M_{GT}^2} \tag{3}$$

The constants $R = \left(\frac{C_A}{C_V}\right)^2$ and K may be derived from the decay data of $O^{14} \longrightarrow N^{14*}$ and the neutron, and have the values $R = 1.40 \pm 0.10$† and $K = (6 \pm 0.02) \times 10^3$ sec (16,17,18). For the case of a small Fermi to Gamow-Teller matrix element ratio, $Y = \frac{C_V\ M_F}{C_A\ M_{GT}}$, and with M_{GT} taken to be positive, Equation 3 assumes the form

$$M_F = -Y \left(\frac{K}{ft}\right)^{\frac{1}{2}} \tag{4}$$

---

†However, see (3, p. 790).

Recent experimental evidence on weak interactions is in accord with the two-component theory of the neutrino revived independently by Salam (19), Landau (20), and Lee and Yang (21). Whereas both the neutrino and antineutrino are thought to be chargeless, without rest mass, and with spin $\frac{1}{2}$, their distinction was first introduced as a result of the Dirac theory which requires both neutral and charged particles to have antistates. The verification of nonconservation of parity in beta decay strongly supports the hypothesis of a distinction between the two particles on the basis of helicity; that is, the type of neutrino emitted in positron (electron) decay has spin direction antiparallel (parallel) to its momentum direction and therefore has left-handed (right-handed) helicity. In accordance with lepton conservation (22), Lee and Yang (21) suggested that antineutrinos are emitted with electrons and neutrinos are emitted with positrons.

The two-component theory requires that the parity conserving and nonconserving coupling constants be equal in magnitude, $C_x = \pm C_x'$. Evidence for further simplification of coupling constants is presented in Table 1.

The dominantly (V-A) interaction will be assumed in this work although the experiments in Table 1 do not preclude a small mixture of (S,T) interaction. Such a (V-A) interaction is summarized by

$$C_x = C_x' \qquad \text{and} \qquad C_T = C_S = C_P = 0. \tag{5}$$

The presently accepted (V-A) form of the beta-decay Hamiltonian, proposed independently by several authors, was thought to apply not only to nuclear beta decay but to other Fermi interactions such

Table 1. Experimental evidence concerning beta-decay coupling constants

Result	Reference	Experiment
$C_T = 0$ and or $C_A = 0$ $C_S \neq 0$ and or $C_V \neq 0$	(23)	Existence of pure Fermi transitions
$C_S = 0$ and or $C_V = 0$ $C_T \neq 0$ and or $C_A \neq 0$	(23)	Existence of pure G-T transitions
$C_V \gg C_S$, $C_V' \gg C_S'$	(24)	A^{35} ($\beta^+ - \nu$) angular correlation
$C_A \gg C_T$, $C_A' \gg C_T'$	(25)	He^6 ($\beta^- - \bar{\nu}$) angular correlation
	(26)	$\bar{\nu}$ helicity from Eu^{152m} electron cap.
	(27)	Li^8 ($\beta^- - \alpha$) angular correlation
$C_V / C_A \approx -1$ Coupling constants real	(28)	Beta decay of polarized neutrons
$C_A \approx C_A'$, $C_V \approx C_V'$	(2)	Beta asymmetry from polarized nuclei
	(29)	$\beta - \gamma$ circular polarization corr.
	(30)	Longitudinal polarization of β - rays

as muon decay and muon capture (31,32,33). A universal interaction strength was indicated by the unexpected similarity between the vector coupling constants in beta and muon decay (34). It was felt that compared to the vector coupling coefficient of the muon which posseses no strong couplings, the beta-decay vector coupling coefficient should be considerably altered because the nucleon undergoing beta decay is strongly coupled to virtual pions. To explain the near equality between vector coupling constants Feynman and Gell-Mann (33) postulated a conserved vector current (CVC) operating in beta decay in analogy with electrodynamics. This attributed the beta interaction strength not only to the bare nucleons but also to the virtual pions. The results of several difficult experiments (35) are all in agreement with the predictions of the CVC theory of beta decay. However, according to Blin-Stoyle (36) it is not clear that the experiments are inconsistent with a theory in which the axial-vector current is not conserved.

An uncertainty in the CVC theory remains in the considerable deviation of experimentally determined values of C_A/C_V from each other (3, p. 790) and from -1. Consequently, the numerical value of C_A/C_V will be left unspecified in this work.

B. Experiments Concerning Parity Nonconservation in Nuclear Beta Decay

1. Beta asymmetry from polarized nuclei

The violation of parity in beta decay was first demonstrated experimentally by Wu et al. (2) following the historic suggestion made by Lee and Yang (1). The angular distribution of electrons emitted from polarized Co^{60} nuclei was examined. Electrons were found to be emitted pre-

ferentially in a direction opposite that of the nuclear spin. A precise value for the asymmetry was not obtained. Such work on oriented nuclei is limited, however, in that only a few sources can be aligned, directional measurements are not easily done with beta counters in cryostats, and the method is not sensitive enough to determine precise magnitudes of parity violation. (Interesting work had been done on oriented Co^{60} prior to that of Wu. See (37) for example).

2. Longitudinal polarization of beta rays

Important contributions to parity nonconserving beta-decay theory have been made through two general types of polarization measurements using unoriented sources. The degree of longitudinal polarization of beta rays (positrons) has been determined to within 10% or better to be -(+) v/c, the velocity of the beta ray relative to the velocity of light. This is in good agreement with maximum parity violation predicted by the two-component neutrino theory. A complete summary of measurements of the longitudinal polarization of beta rays has been made by Kofoed-Hansen and Christensen (30, p. 66).

3. Beta-gamma circular polarization correlation experiments

Similar and further information has been obtained in measurements of the circular polarization of gamma rays emitted at an angle θ relative to the beta momentum direction in the decay of an unpolarized source (29, 38). Because of parity nonconservation, more electrons are emitted antiparallel to the initial nuclear spin. Therefore, the determination of the direction of beta emission from an unoriented source preferentially se-

lects daughter nuclei with spins oriented relative to the beta momentum. The gamma rays emitted from these nuclei at an angle $\theta \neq \pi/2$ have a non-zero degree of circular polarization because of conservation of angular momentum in electromagnetic interactions.

As is the convention in quantum mechanics, the degree of polarization of gamma rays is defined relative to the two pure states "right circularly polarized", in which the electric vector describes a circle and rotates clockwise for an observer looking in the direction of the photon momentum and "left circularly polarized", in which the electric vector rotates counterclockwise so that the spin direction is antiparallel to the photon momentum. The degree of circular polarization P_c is defined by $P_c = \frac{N_R - N_L}{N_R + N_L}$, where N_R and N_L are the intensities of photons with pure right or pure left circular polarization, respectively. With this definition $P_c = +1$ for pure right circularly polarized photons, $P_c = 0$ for an unpolarized beam, and $P_c = -1$ for pure left circularly polarized photons.

4. Information to be gained from beta-gamma circular polarization experiments

For allowed transitions the angular distribution of circularly polarized gamma rays emitted at an angle θ relative to the preceding beta particle is given by (4,5)

$$W(\theta, \tau) = 1 + \tau A \, v/c \cos\theta ,$$

where v/c is the velocity of the beta ray relative to the velocity of light, $\tau = +1$ (-1) for right-handed (left-handed) circularly polarized photons, and A is the asymmetry parameter for which theoretical expres-

sions have been given by several authors (4,5,39,40). The experimentally measured quantity is thus

$$P_c = A\, v/c \cos \theta \quad , \tag{6}$$

the degree of circular polarization of the gamma rays.

Equation 6 will be used in the present study to obtain information about certain beta transitions; its verification will now be discussed. The $\cos \theta$ dependence of the gamma polarization has been well established (41,42). Moreover, in measurements on Co^{60}, Steffen (41) determined the v/c dependence of the polarization down to about 100 keV ($v/c \approx 0.5$). He obtained a pure v/c dependence to within 10% experimental error. The question is not completely settled because of experimental difficulties encountered for values of v/c less than 0.5.

The assumptions of the (V-A) interaction lead to a simple form of A for the case of pure G-T transitions like Co^{60} and Na^{22}. For Co^{60} the theoretical value (4) is $A = -1/3$ and for Na^{22}, $A = +1/3$. The best data agree to within 5-7% of the theoretical prediction. Appel (43), for example, obtained $A = -0.335 \pm 0.018$ for Co^{60} and $A = +0.295 \pm 0.054$ for Na^{22}. It should be noted that this constitutes very good evidence for maximum parity violation.

The correlation parameter A for mixed transitions is dependent on the following:

(1) The spins of the initial and final nuclear states;

(2) The multipole order L of the gamma rays;

(3) The gamma-ray multipole admixture ratio of 2^{L+1}- pole to 2^{L} - pole radiation;

(4) The Fermi to Gamow-Teller matrix element ratio, $Y = \frac{C_V M_F}{C_A M_{GT}}$. Measurements of the asymmetry parameter A in some cases have yielded strong evidence supporting specific spin assignments (44,45,46). In other cases the gamma-ray multipole ratio has been obtained (47,48,49). Finally, the asymmetry parameter has been measured in mixed Fermi and Gamow-Teller transitions for which the spins and parities of the nuclear states are known, in order to obtain the Fermi to Gamow-Teller matrix element ratio (41,48,50,51,52). The last is the objective of the present investigation.

C. Previous Beta-Gamma Circular Polarization Measurements

The agreement among various measurements on mixed transitions has generally not been complete. In their earlier work on Na^{24}, Sc^{44}, Sc^{46}, V^{48}, Co^{58}, and Mn^{52}, Boehm and Wapstra (50,53) obtained results suggesting the presence of significant interference between Fermi and G-T couplings, particularly in the case of Sc^{46}. Results obtained in more recent measurements by Bloom et al. (48,54) at Livermore and by Daniel et al. (51) at Heidelberg have strongly disagreed with the conclusions reached by Boehm. The work of the Livermore group has been extensive including not only the above radioisotopes but also Ar^{41}, Co^{56}, Fe^{59}, Zr^{95}, Nb^{95}, and Cs^{134} (44, 45). They obtained values of A consistent in all cases with a small or vanishing Fermi contribution. The Livermore results, however, have conflicted with those of many others (41,50,53,55,56,57,58,59,60). In one of the few exceptions, agreement between various groups in the case of Na^{24} was good.

The most controversial case, Sc^{46}, has been thoroughly investigated by several groups. Boehm and Rogers (56) re-examined this decay and obtained values of the asymmetry parameter consistent with a large Fermi contribution in fair agreement with Steffen (41) and Jungst and Schopper (58). Boehm and Rogers interpreted some of their measurements as a strong time-dependent attenuation of the circular polarization in certain chemical compounds of scandium. The Livermore group measured Sc^{46} in 7 different chemical and physical forms (61). They found a small Fermi contribution and no evidence for chemical attenuation effects. This was in good agreement with their earlier work and with the results of an investigation of 15 different scandium sources done by Daniel and co-workers (52) at Heidelberg. The Heidelberg group has also done considerable work on mixed transitions and in most cases has obtained results in agreement with those of the Livermore group (51,60,62). However, Singru and Steffen (59) subsequently obtained a value of A tending to substantiate the earlier work of Steffen (41) and that of Boehm and Rogers but without observing attenuation effects as did the latter. Thus the discrepancy between the various scandium results has not been completely explained.

More recent experiments on Na^{24} and Al^{24} by Haase et al. (63) and by Bloom et al. (64) have indicated that the theoretical estimate of Bouchiat (65) for the Fermi matrix element of Na^{24} was too high and probably not reliable. The difficult Al^{24} measurements, some of only a few done on short lived isotopes (46,66), were undertaken to provide evidence for the CVC theory of beta decay. The results of the two experiments were in agreement with each other and with the calculations for the magnitude of the Fermi matrix elements made by Blin-Stoyle and Novakovic

(with the assumption (16) of a few percent charge-dependent nuclear force suggested by the latter). However, because of the small magnitude of the meson exchange contribution calculated assuming conventional beta-decay theory, the measurements were not sensitive enough to determine whether or not the vector current is conserved. Bloom *et al.* estimated that a reduction of the experimental error by a factor of 5 would be necessary to differentiate between the small meson exchange contribution calculated assuming the conventional theory and the zero contribution of the CVC theory.

A survey of experimental results, including several not discussed here, has been made by Estulin and Petushkov (29).

D. Motivation for the Experiment

Several considerations led to the selection of Sb^{124} and Cs^{134} for investigation. The correlation measurement requires a decay scheme such that coincidences between the beta and subsequent gamma rays in the transition of interest can be reasonably separated from competing events. Also, experimental difficulties hinder the detection of beta energies below 100 keV. The long counting times necessary for these experiments make measurements on short lived isotopes difficult. Moreover, the production of isotopes with short half-lives requires a facility such as a cyclotron; only a few of these isotopes have been attempted. A complex situation exists for first-forbidden transitions in which several matrix elements may contribute (67,68). It was decided to consider only allowed transitions.

With these limitations in mind, a survey of isotopes yielded allowed transitions in Cs^{134} and Sb^{124} for which little beta-gamma circular polarization information was available. No Cs^{134} results had been published when these measurements were initiated and apparently only two results have been published since then (44,60). A third cesium measurement was warranted because agreement between these two measurements was not complete. Results for the allowed transition in Sb^{124} have been reported only once previously (69). In view of the poor agreement existing between measurements in other cases (examples of which have been discussed in Section C) another antimony measurement was thought to be desirable.

In addition, these cases are of particular interest since they occur in the medium mass region where charge dependent effects in the nucleus may significantly influence the Fermi to Gamow-Teller matrix element ratios (16). Apparently no calculations of Fermi and Gamow-Teller matrix elements have been published for these transitions; however, an accumulation of experimental data concerning beta decay matrix elements may provide useful information to nuclear theorists.

II. EXPERIMENTAL INVESTIGATION

A. Selection of the Method

The quantity measured in this investigation was the degree of circular polarization of gamma rays emitted at an angle θ relative to the direction of the coincident beta momentum. The direction and energy of beta rays was determined with a beta scintillation spectrometer. The measurement of the circular polarization of gamma rays will now be discussed.

A comparison of the possible ways for measuring the circular polarization of gamma rays has been made by Schopper (70). Of the methods which could utilize the interaction of gamma rays with polarized matter, the photoelectric effect has found little application since this process involves the ejection of electrons by incident gamma rays mainly from inner shells where the electrons cannot be polarized. Pair production might be used for photon energies above 5 MeV where this effect is dominant. Apparently, no detailed calculations have been attempted, however. The same is true for the photonuclear effect which might be used at energies above 10 MeV. Thus for photon energies between 0.2 and 10 MeV Compton scattering from polarized electrons available in magnetized iron is the only method which has been widely used (29).

Polarization measurements utilizing the spin dependence of the Compton cross section use one of three types of geometries; transmission, backscattering (through angles between $\pi/2$ and π), and forward scattering (through angles $< \pi/2$). The transmission method has been used for circular polarization measurements by many authors (26,47,57). The quantity measured was the difference in photon transmission through iron polarized

parallel and antiparallel to the direction of incident photons. Of the three geometries the transmission energy discrimination is usually best; but counting rates are quite low, and it is difficult to determine the effective length of the iron absorber.

To measure the circular polarization of photons with energies less than 500 keV, Steffen (71) has used Compton backscattering through large angles (average = 125°). Compared to forward scattering the observed effect for back angles is larger in magnitude for lower energies, but it decreases with increasing photon energy. Between 0.6 and 2 MeV better energy resolution and a larger observed effect may be obtained using forward scattering. Consequently the forward Compton scattering method was selected for this investigation.

B. Description of the Measurement

From Equation 6, the degree of circular polarization P_c of gamma rays emitted at an angle θ with respect to the direction of beta momentum is given by $P_c = A\ v/c \cos\theta$ for electrons. The measurement of the circular polarization of gamma rays following nuclear beta decay therefore consists of selecting beta-gamma coincidences with a fixed angle θ between the directions of beta-ray and gamma-ray emission and simultaneously detecting the circular polarization of the gamma ray. The degree of polarization was measured by observing the intensity of photons Compton scattered from magnetized iron for opposite orientations of the electron spin $\underline{S}$.

As illustrated in Figure 8, (p. 52) beta rays were detected by a scintillation crystal placed close to a radioactive source (a beta ray emitted from the point source at an angle β relative to the crystal axis

is shown entering the crystal). The gamma ray emitted at the angle θ with respect to the direction of the preceding beta was scattered from the region of partially polarized electrons in the magnet. The direction of the incident photon momentum $\underline{k}_o$ was roughly 30^o relative to the electron spin $\underline{S}$. The scattered gamma ray with momentum $\underline{k}$ was detected by a NaI(Tl) scintillation crystal.

Electronic circuits were used to record the occurrence of coincidence events detected by the beta-ray and gamma-ray spectrometers. Each spectrometer consisted of a scintillation crystal viewed by a photomultiplier tube. Beta-ray and gamma-ray energy selection was done in separate channels by subjecting the respective photomultiplier pulses to amplitude analysis. Single channel analyzers were employed, the outputs of which were monitored in scalers. Coincidence events satisfying the energy requirements were accumulated in separate banks of scalers for opposite orientations of the scattering magnet. The magnet orientation was reversed by changing the direction of current in the magnetizing coils. The control of operations such as reversing the magnet and changing scaler banks was done with an automatic cycling system.

The asymmetry parameter A was determined from the relative difference in coincidence counting rates for opposite orientations of the magnet. The average v/c of the detected beta rays was determined from the beta pulse height discriminator levels and from the theoretical beta spectrum. Furthermore, the raw coincidence asymmetry was corrected for background coincidence events for which the coincidence asymmetry was zero. The percentages of background coincidence events (such as gamma-gamma coincidences, etc.) were determined in separate experiments.

C. Description of the Apparatus

In this section the geometrical arrangement and associated electronic circuitry used in this investigation will be described in further detail. As illustrated in Figure 1 the geometrical arrangement consisted of the radioactive source and the beta spectrometer, which was used to determine both the direction of emission and energy range of the beta rays. The scattering magnet and gamma-ray spectrometer were used to measure the circular polarization of gamma rays.

1. Circular polarization analyzer

The gamma-ray circular polarization analyzer utilized forward Compton scattering from polarized electrons available in a cylindrical magnet. Gamma rays from a source located on the central axis were scatter from the inner cylinder of the magnet through an average angle of 56° and were detected by a 3" x 3" NaI(Tl) crystal. Approximately 8% of the electrons in the Armco iron scattering cylinder were polarized when it was magnetically saturated. The direction of the electron polarization could be reversed by reversing the current in the solenoidal magnetizing coils. The angular spread of the gamma rays was defined by the lead collimating system. In this geometry a large angular spread and cylindrical symmetry were used to provide a large solid angle of detection. Gamma rays were prevented from going directly to the crystal by the central lead absorber which was axially centered and suspended from a thin beryllium disk. Undesirable scattering of gamma rays from the unpolarized electrons in the copper coils was not significant in this system due to the thickness of the scattering magnet wall (one inch).

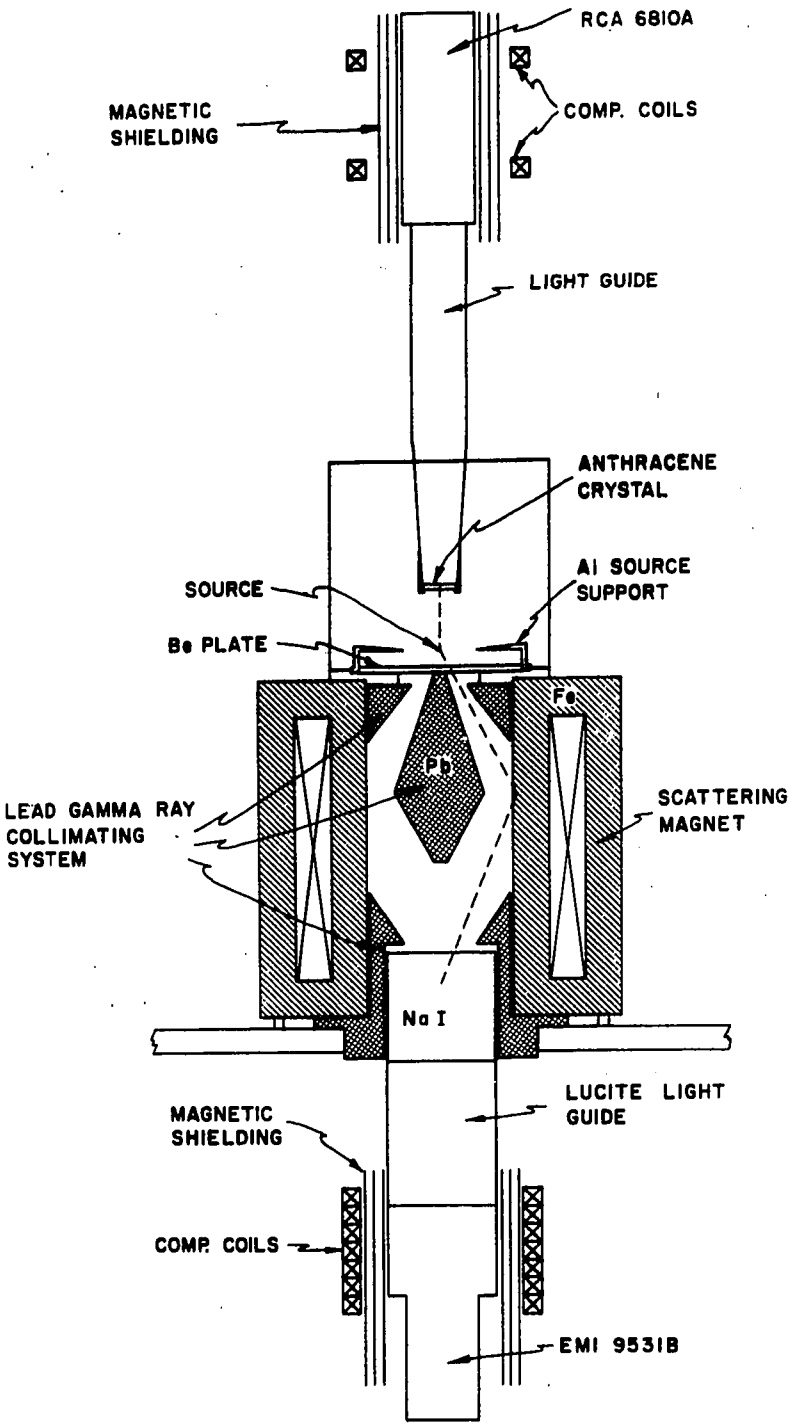

Figure 1. Experimental arrangement used for the measurement of beta-gamma circular polarization asymmetry parameters

2. Beta-ray and gamma-ray spectrometers

The direction of beta momentum was defined by a 1" diameter anthracene scintillation crystal located on the central axis near the source. The anthracene was sufficiently thick (1/8th") to stop beta rays with energies less than 800 keV. The crystal was optically coupled with clear, high-viscosity silicone grease to a Lucite light guide. The resolution of the beta spectrometer was found to be improved by covering the entrance crystal face with thin aluminized Mylar foil. The 0.9 mg/cm^2 Mylar served to decrease the loss of scintillation light without absorbing incident beta rays appreciably. Room light was kept from the crystal by a 10 mil aluminum house which was 6" in diameter. Scattering of beta rays from the housing was reduced by lining it with 10 mil Plexiglas sheet and by collimating the beta rays entering the crystal.

Scintillations from the anthracene were transmitted to a 14 stage RCA 6810A photomultiplier tube by means of a Lucite light guide. This was a polished $1\frac{1}{2}$" diameter rod 10" long and tapered at the lower end to accomodate the anthracene. The light guide allowed the magnetically sensitive phototube to be located at a distance from the magnet. The influence of the stray field of the analyzer magnet on the phototube was further reduced by surrounding the tube with several layers of Netic and Co-Netic magnetic shielding foil and by using a Helmholtz compensation coil, the field of which was reversed along with that of the analyzer magnet. Nearly complete cancellation of fields was obtained at the phototube. With the above conditions the resolution of the beta-ray spectrometer was 15% for the 624 keV internal conversion line of Cs^{137}.

The gamma-ray spectrometer consisted of a 3" x 3" NaI(Tl) crystal coupled to an 11 stage EMI 9531B photomultiplier tube by means of a Lucite light guide 5" in length. For operation at this distance from the magnet, the phototube was enclosed by a Mu-metal shield in addition to several layers of Netic and Co-Netic foil. The solenoidal compensation coil used for this phototube had to be carefully adjusted because of the larger stray field present. The advantage of this spectrometer over one using a very long light pipe was improved resolution; however, this arrangement had the disadvantage of requiring periodic checks on the effects of the magnetic field on the phototube. The resolution of this spectrometer for the 662 keV gamma rays of Cs^{137} was 11%.

3. Electronics

Shown in Figure 2 is a block diagram of the electronic circuitry used in this investigation to detect and record beta-gamma coincidences, to perform beta-ray and gamma-ray energy analysis, and to automatically control the accumulation of data.

a. Circuitry for coincidence selection and energy analysis A fast-slow coincidence circuit configuration was used. With this arrangement the fast coincidence circuit was triggered upon the arrival of a pulse from each of the phototubes within an interval of time less than its "coincidence resolving time". Amplitude analysis of the beta and gamma pulses was meanwhile performed in separate channels. The fast coincidence circuit output pulse was delayed until the slower pulse height analyzers had time to respond. The delayed pulse was then placed in slow coincidence with the analyzer outputs. A signal from the slow triple

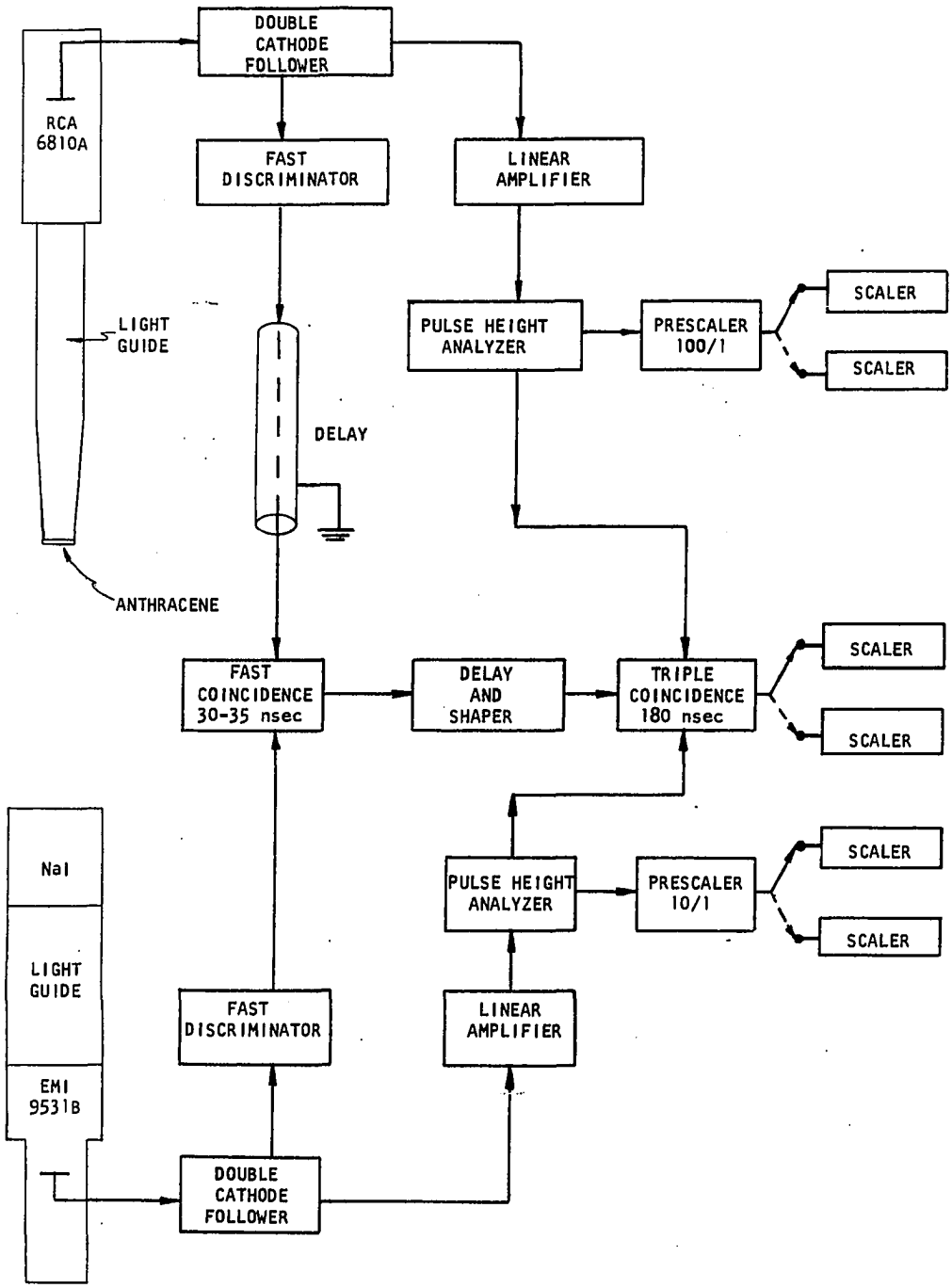

Figure 2. Block diagram of the electronic circuitry

coincidence circuit was thus fed to an appropriate scaler when the two phototube pulses had satisfied the energy requirements and had triggered the fast coincidence circuit.

In detail, a signal appearing at the anode of the RCA 6810A photomultiplier tube was proportional in amplitude to the light output of the anthracene crystal and thus was proportional to the energy of the detected beta ray. Anode pulses were fed in parallel to the fast and slow beta channels. A one megohm anode load resistor was used to obtain the 100 μsec pulse decay time suitable for the linear amplifier in the slow channel. A cathode follower located near the phototube provided isolation from the fast channel and matched the high anode load impedance to the low impedance of the coaxial cable leading to the amplifier.

Anode pulses were fed to a fast discriminator, physically located close to the phototube, through the other cathode follower. To prevent multiple triggering the width of the input pulses to the fast discriminator was reduced to 1 μsec by RC clipping. This discriminator was composed of two tunnel diode univibrator circuits of the Whetstone design (72). The input univibrator was adjusted to trigger on any pulse which just exceeded the noise level of the phototube. The second univibrator, acting as an isolation stage, was set to trigger on the output of the first. Thus a standard pulse was obtained from the discriminator which was related in time to a very early point on the leading edge of the anode pulse. The same type of fast discriminator was used for signals appearing at the anode of the gamma phototube. Output pulses from the beta fast discriminator were delayed about 50 nsec in a coaxial cable in order to be synchronized with output pulses from the gamma fast discriminator.

The difference in timing was due to the slower rise time of the gamma-ray pulses from the NaI crystal (250 nsec) as compared to the rise time of pulses from anthracene (30 nsec).

The gamma fast discriminator output pulses were shaped to approximately 30 nsec width and added to the much narrower pulses from the beta fast discriminator at the input to a tunnel diode univibrator which served as the fast coincidence circuit. The univibrator was set to trigger on the sum of the two discriminator inputs. The performance of the fast coincidence circuit will be discussed later.

Pulses were amplified in the beta slow channel by a Hamner Model N-380 transistorized linear amplifier. The amplifier employed double delay line clipping and its bipolar output was fed to a Hamner Model N-685 jitter-free pulse height analyzer. The analyzer gave an output for every input pulse whose amplitude exceeded a selected lower level but was less than a selected upper level. The output was conveniently related in time to the bipolar input pulse cross-over point. The trigger pulse from the beta pulse height analyzer was fed to a Hamner coincidence module Model N-681. Energy analysis was performed in the gamma slow channel in the same way with similar Hamner modules. Output pulses from the fast coincidence circuit and the pulse height analyzers were synchronized by using suitable delays and fed to the triple coincidence circuit. The Hamner coincidence module was operated at a resolving time of 180 nsec.

Coincidence counts were registered in two RIDL Model 49-30 scalers, one for each polarization direction of the analyzer magnet. The output of the beta pulse height analyzer was monitored by two Tracerlab Model Sc-75 scalers after having been prescaled by a factor of 100 in a Hew-

lett Packard Model 520A high speed scaler. Similarly, gamma singles counts in the selected energy range were prescaled in a RIDL 1 megacycle decade unit and were recorded in either of two RIDL Model 49-30 scalers.

b. Automatic cycle control Data was obtained nearly 24 hours per day using an automatic cycle control system. Counts were accumulated alternately in separate banks of scalers for opposite current directions of the scattering magnet. An accurate timer utilizing a 100 kc crystal controlled oscillator was used to control the 32 sec intervals during which counts were recorded in either bank of scalers. Between counting periods the magnet and compensation coil currents were reversed and scaler banks were changed by means of a set of cam operated switches.

In detail, the sequence of operations was as follows: With the magnet oriented in a given direction the appropriate scalers were switched on electronically, and the interval timer was simultaneously started. At the end of 32 sec the interval timer gated off the scaler inputs and started a 1 rpm motor controlling the operations between counting periods. After a 0.75 sec delay the magnet was turned off by a cam operated microswitch. Immediately a second microswitch activated the magnet reverse relay, reversed the current in the phototube compensation coils, and changed banks of scalers. The magnet was then turned on by release of the microswitch. Four seconds later a counting period was started during which the magnet was in its second orientation. Following the counting period the intermediate sequence of operations returned the system to its original condition and the cycle was repeated.

4. Sources

The isotopes Co^{60}, Sb^{124}, Cs^{134}, and Cs^{137} were obtained from Oak Ridge National Laboratory in the form of high specific activity cloride solutions. The mercury source material was $Hg(NO_3)_2$ in HNO_3 solution. The Na^{22} was obtained from Nuclear Science Engineering Corporation as a cloride.

Sources were deposited by solution evaporation on 0.9 mg/cm^2 aluminized Mylar film. Ordinarily only about one drop of about 2 or 3 μLiters from a 5 μLiter pipette was sufficient. Prior to deposition the Mylar was stretched across a thin aluminum ring of inside diameter 1-1/8" and cemented with Eccobond-26.

Several sources were made for each isotope. From these a few were selected which best met the requirements of uniform thickness with diameter less than 0.2" and source strength between 80 and 90 μC. The Na^{22} source used for calibrating the gamma spectrometer was deposited in the center of a 1/8" thick plastic disk.

The sources were examined for radioactive contaminants using the gamma scintillation spectrometer and a multichannel pulse height analyzer. No contamination was detected.

D. Performance Tests

The electronic circuitry used in this investigation was required to have good stability because of the small magnitude of the observed effect (less than 1%) and the long counting times needed for reasonable statistical accuracy. Consequently stability tests were made before and concurrent with the accumulation of data.

1. Interval timer and counting system

The performance of the interval timer which gated the scalers was checked periodically. For the standard test a one megacycle output from a Tetronix type 181 time marker generator was fed to the beta prescaler. The output from the prescaler was gated by the interval timer. The relative difference in counts accumulated alternately in the two scalers for several hundred cycles was typically $2 \times 10^{-8}\%$. Both the short and long term changes in the timed interval were small. A drift of only $3.7 \times 10^{-4}\%$ occurred in the 32 sec counting time during a 7 month period.

The performance of the four RIDL scalers was checked with an E-H Research Laboratories Pulse Generator Model 120D. Parallel outputs from this pulse generator were fed to each pair of scalers. The scalers were gated on and off and alternated by the automatic program control system. In a typical test input pulses with a frequency of 4 kc were counted overnight. The largest difference in total counts between any two of the four scalers was $3 \times 10^{-4}\%$. Part of this difference could have been due to a noticable dependence of repetition rate on room temperature for this particular pulse generator.

2. Single channel pulse height analyzers

After the performance of the scalers and timing system was found to be satisfactory, the beta and gamma pulse height analyzers were tested. Changes in Co^{60} counting rates were observed due to pulse amplitude dependence on ambient temperature, short-term gain dependence on source strength, and long-term gain drifts.

Each channel exhibited counting rate variations with ambient temperature due to the combined temperature dependence of the linear amplifier, phototube, and detecting crystal. The Hamner linear amplifier gain stability was rated at better than 0.1%/°C. The phototube-crystal combination was not this good. Short-term variations in Co^{60} counting rates were reduced to 0.4% for the gamma channel and 0.25% for the beta channel by, among other things, controlling the room air conditioner from a point near the apparatus. There was, however, a 2°C cyclic variation about the average temperature with a period of approximately 15 min. The effects of this variation could be tolerated since the period was long compared to the 32 sec switching time of the magnet.

At the counting rates used, short-term gain changes with source strength were not serious. Beta counting rates were between 3×10^4 counts/sec and 4×10^4 counts/sec. Gamma counting rates were 7×10^3 to 9×10^3 counts/sec for Co^{60} and Cs^{134}, and 24×10^3 counts/sec for Sb^{124}. After a change of sources, stability was usually obtained within $\frac{1}{2}$ hour. Measurements were started after waiting 1 to $1\frac{1}{2}$ hours.

Both channels exhibited a gradual drift in counting rates. The drift in the beta channel was thought to be due mainly to long-term variations in the output of the high voltage supply. This was an NJE Corporation Model S-325 supply with long-term stability rated better than 0.1% per 8-hour day. All power supplies, amplifiers, etc., were operated from line voltage regulated by a Stabiline Model IE 5105 voltage regulator under constant load conditions. The high voltage supply used for the gamma channel was a Smith Florence Model 120 (0.03% stability/day) for cesium measurements and a Keithley Model 242 (0.01% stability, indef-

initely) for the antimony measurements.

It was concluded from the stability analysis of the energy selection channels that the long-term drift could be tolerated for a period of about 10 days. The drift was gradual enough to obtain reasonable averages of experimental quantities over this interval from the analysis of calibrations taken before and after the 10 day period.

A systematic difference in count accumulation was noted during the initial testing of the system, and was attributed to the differences in dead times of the scalers. This effect was made negligible by using the common 100/1 prescaler in recording beta counts and the common 10/1 prescaler in recording gamma-ray counts.

3. Coincidence circuits

The performance of the tunnel diode fast coincidence circuit was checked periodically. A typical resolving time curve for coincidences between beta and gamma rays of Co^{60} is shown in Figure 3. There was little change in coincidence counting efficiency over a 10 day period when resolving times of 30-35 nsec were used. The coincidence resolving time had a tendency to increase slightly with time, probably due to long-term drift in the Sorenson Model QB12-1 low voltage DC supply used to provide the reference voltage for the tunnel diode circuit. Such changes were found to occur only very slowly and were adequately accounted for by frequently checking the random coincidence rate (which varied directly with the coincidence resolving time).

A Hamner coincidence module Model N-681 was used as a triple coincidence circuit. All three inputs exhibited very little time jitter compared to the 180 nsec resolving time at which this unit was operated. It

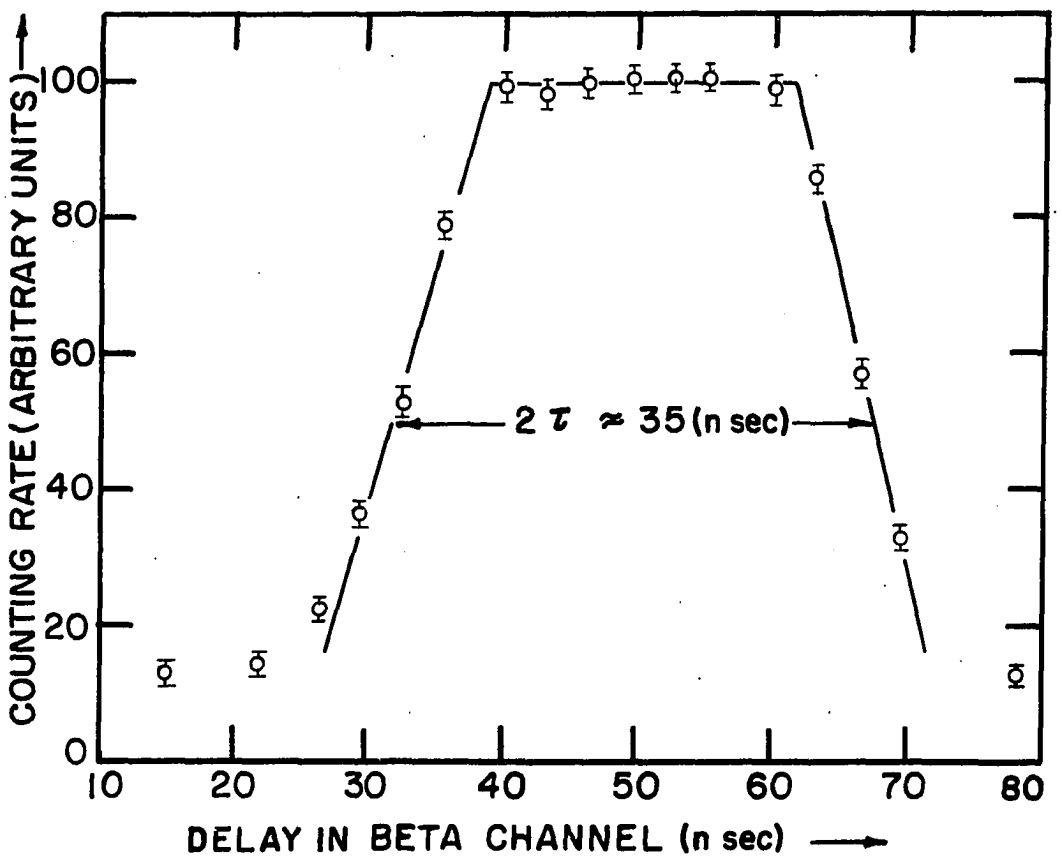

Figure 3. Typical beta-gamma coincidence resolving time curve for Co^{60}. The triple coincidence counting rate is shown as a function of delay in the beta fast channel

was found that the counting efficiency did not change until the resolving time was lowered to approximately 70 nsec. Essentially no adjustment of the coincidence circuit was necessary throughout the investigation.

4. Magnet stray field effect on photomultiplier tubes

A Helmholtz coil was used around the beta phototube as illustrated in Figure 1 to cancel the stray field of the analyzer magnet at the phototube. By daily adjustment of the coil current, differences in the beta detector counting rates for opposite directions of the analyzer magnetic field were reduced to less than 0.02% (less than 0.01% for most measurements). Only about 15 ampere-turns were needed for good compensation. Both the current-regulated power supplies used for the compensation coil and the analyzer magnet were designed and built by the Ames Laboratory Instrument Group and had better than 0.05% / day current regulation.

Being nearer the magnet, the gamma-ray phototube was more sensitive to the stray field effect. A solenoidal coil of about 65 ampere-turns was needed for compensation. A Power Designs Model 4005 current regulated supply with a rated stability of better than 0.1% / day, was used to supply the coil current. Daily adjustments resulted in gamma counting rate differences usually less than 0.015% and rarely greater than 0.03%.

Tests showed that the stray field of the magnet was established in less than one second. This indicated that the 4 sec magnet turn on time was sufficient to ensure saturation before counts were recorded.

When adequate stability of the electronic circuitry has been obtained, several series of runs were made using Co^{60}, Cs^{134}, and Sb^{124} sources. The experimental procedures used will be described next.

E. Experimental Procedure

1. Measurements of the raw coincidence asymmetry

Several long series of runs were made to determine the raw coincidence asymmetries for Co^{60}, Cs^{134}, and Sb^{124}. Since measurements were made relative to cobalt as a standard, Co^{60} sources were run before and after the Cs^{134} series as well as before and after the Sb^{124} series. Sources were changed approximately every 10 days to reduce possible dependence of results on any given source. The counts accumulated in the beta, the gamma, and the coincidence scalers were recorded every 12 hours. After each run the data was checked and, if necessary, slight adjustments of the magnet compensation coils were made.

To eliminate possible systematic errors arising from differences in scalers, i.e., due to differences in dead times, scaler banks were changed after each 12 hour run. In this way the task of recording events associated with a given magnet orientation was shared equally between the two members of each pair of scalers (3 pairs in all). In addition the scaler banks were switched near the middle of each series so that scalers recording events corresponding to a given orientation of the magnet during the day were used during the second half of the series to record such events during the night.

It was necessary to establish the random coincidence rate, and the gamma-gamma coincidence rate, as well as to set the beta and gamma pulse height analyzer windows before each series was started. Consequently the following procedure was adopted. The gamma-ray spectrometer was calibrated by directly exposing the NaI crystal to Hg^{203}, Na^{22}, and Cs^{137} sources. The pulse height spectra from each of these sources was re-

corded using a 256 multichannel analyzer (Nuclear Data Model ND 102). The channel number corresponding to zero energy was located using an RIDL Model 47-2 pulse generator, and at the same time the linearity of the linear amplifiers and the analyzer was checked. The beta spectrometer was then calibrated as discussed later. Sufficient time was allowed for phototubes to adjust to each calibration source prior to recording the spectra. After positioning the source whose coincidence asymmetry was to be measured, the beta and gamma energy discriminator levels were set with the aid of the calibration data. Pulse height spectra observed by gating the multichannel analyzer with one or the other single channel analyzers were used for this alignment.

The fast discriminators were then adjusted and the alignment of the triple coincidence circuit was checked. A coincidence resolving time curve was obtained by plotting the coincidence counting rate as a function of the delay in the beta fast channel. The delay was changed by inserting various measured lengths of coaxial cable between the beta fast discriminator and the fast coincidence circuit. The fast coincidence resolving time was adjusted, and the correct beta delay cable length was selected.

The random coincidence rate and the gamma-gamma coincidence rate were determined as discussed in the next paragraphs. The series of runs was then begun to determine the raw coincidence asymmetry.

The above procedure was again followed at the conclusion of the series. In this way the effect of instrumental drifts on the experimental quantities could be adequately determined over the 10 day period.

2. Background coincidences

The raw coincidence asymmetry was corrected for background coincidences for which the asymmetry was zero. These consisted of random coincidences, gamma-gamma coincidences, and coincidences due to gamma rays reaching the crystal without scattering from the region of polarized electrons. Coincidences due to room background and to backscattered beta rays were negligible.

a. Random coincidences The percentage of coincidences due to uncorrelated events was determined by inserting a 100 nsec delay in the gamma channel feeding the fast coincidence circuit. The counting rate observed under these conditions was compared to the total counting rate obtained during the next coincidence asymmetry run. The determination of the random coincidence rate every five days was adequate to ensure a good average over this interval even in the case of Sb^{124} which had a noticeable but gradual decrease in accidental counting rate (because of its 60.3 day half-life). Periodic tests revealed that second order random coincidences could always be neglected. Only an occasional coincidence count was recorded when the input to the triple coincidence circuit from the beta (or alternately from the gamma) pulse height selector was delayed by 500 nsec.

b. Gamma-gamma coincidences The percentage of coincidences between gamma rays resulting from detection of one of the photons by the beta counter was determined for each source by inserting a Plexiglas absorber between the source and the anthracene crystal. The absorber thickness was chosen just sufficient to stop the most energetic electron emitted by each isotope. The counting rate observed under these condi-

tions was the gamma-gamma counting rate since gamma rays freely traversed the Plexiglas. A small 6% correction was applied to the fraction of gamma-gamma coincidences to allow for the change in dead time of the detecting system corresponding to the decrease in the beta channel counting rate when the betas were removed.

c. Coincidences from gamma rays not scattered from polarized material A certain percentage of the gamma rays reaching the NaI crystal were not scattered from the region of partially polarized electrons in the magnet. Instead they reached the crystal by penetrating the central lead absorber or, to a lesser extent, by scattering from the copper coils and from the surface of the collimator system. Such gamma rays resulted in coincidence counts which did not contribute to the coincidence asymmetry. It was thus necessary to correct the raw asymmetry for the percentage of the total coincidence counting rate f_{np} due to gamma rays reaching the crystal without scattering from partially oriented electrons. This background correction was particularly important in this investigation because the photons of cesium and antimony have significantly different energies from those of the standard source, Co^{60}.

The fraction f_{np} was determined for each isotope by comparing scattered gamma-ray pulse height spectra from three different geometries. The gamma-ray spectrum was first obtained with the regular scattering magnet geometry shown in Figure 4a. This was recorded using a multichannel analyzer. A coincidence spectrum was also obtained by gating the analyzer with the triple coincidence circuit. Similar spectra were taken with the geometry of Figure 4b. Here the scattering magnet was replaced by a cylinder of Armco magnet iron. The cylinder had the same

Figure 4. Geometrical arrangements used to determine the fraction of gamma rays scattered from the region of polarized electrons
(a) Scattering geometry
(b) Scattering magnet replaced by magnet core

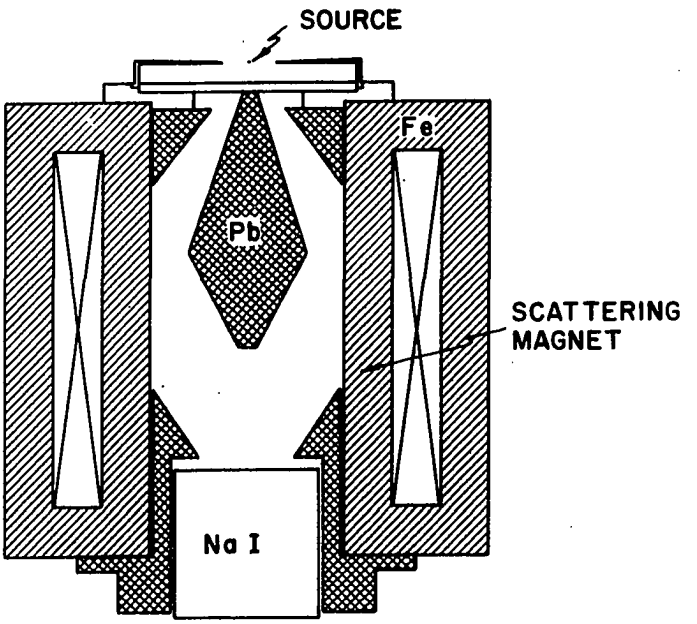
SOURCE
Fe
Pb
SCATTERING
MAGNET
Na I

(a)

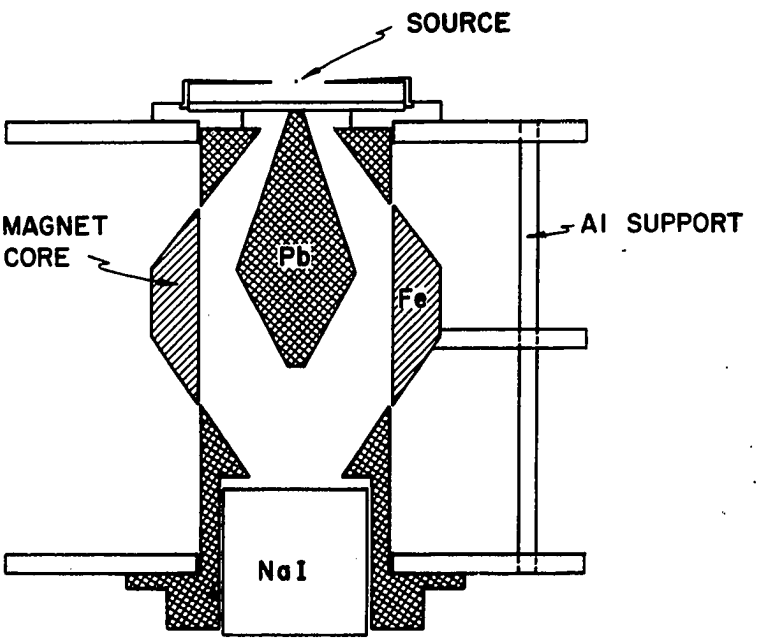
SOURCE
MAGNET
CORE
Pb
Fe
Al SUPPORT
NaI

(b)

dimensions as that part of the polarized region in the analyzer magnet which was exposed to the source. Note that for these measurements the absorber, source holder, and collimating system were positioned just as they were in the regular geometry.

Background spectra were taken with the inner cylinder (magnet core) removed, i.e., with the central absorber and lead collimator system only. This geometry was used to determine the extent to which gamma rays reached the crystal by penetrating the central absorber or by otherwise scattering from the collimating system. By subtracting this background spectrum from that taken with the magnet core plus absorber geometry of Figure 4b the counting rate corresponding to gamma rays scattered only from the region of polarized electrons was obtained. By comparing the resulting net spectrum with that obtained with the regular geometry, the fraction of gamma rays scattered from nonpolarized material was determined as a function of channel number. The portion of these spectra to be included in a correction to a particular raw asymmetry measurement was found from the discriminator levels of the gamma-ray pulse height analyzer.

The response of the gamma-ray spectrometer to the three different geometries is shown in Figures 5, 6, and 7. These spectra have been corrected for slight changes in gain from multichannel analyzer calibrations using Na^{22}, Hg^{203}, and Cs^{137} sources. The calibrations were necessary because long coincidence runs were required for sufficient statistical accuracy. Note that the penetration through the absorber increased with gamma-ray energy as would be expected. Note also the peak common to the magnet core geometry and to the geometry involving only the lead collimating system. This was probably due to scattering from the common

Figure 5. Cs^{134} gamma-ray spectra from three different geometrical arrangements used to determine nonpolarized scattering corrections

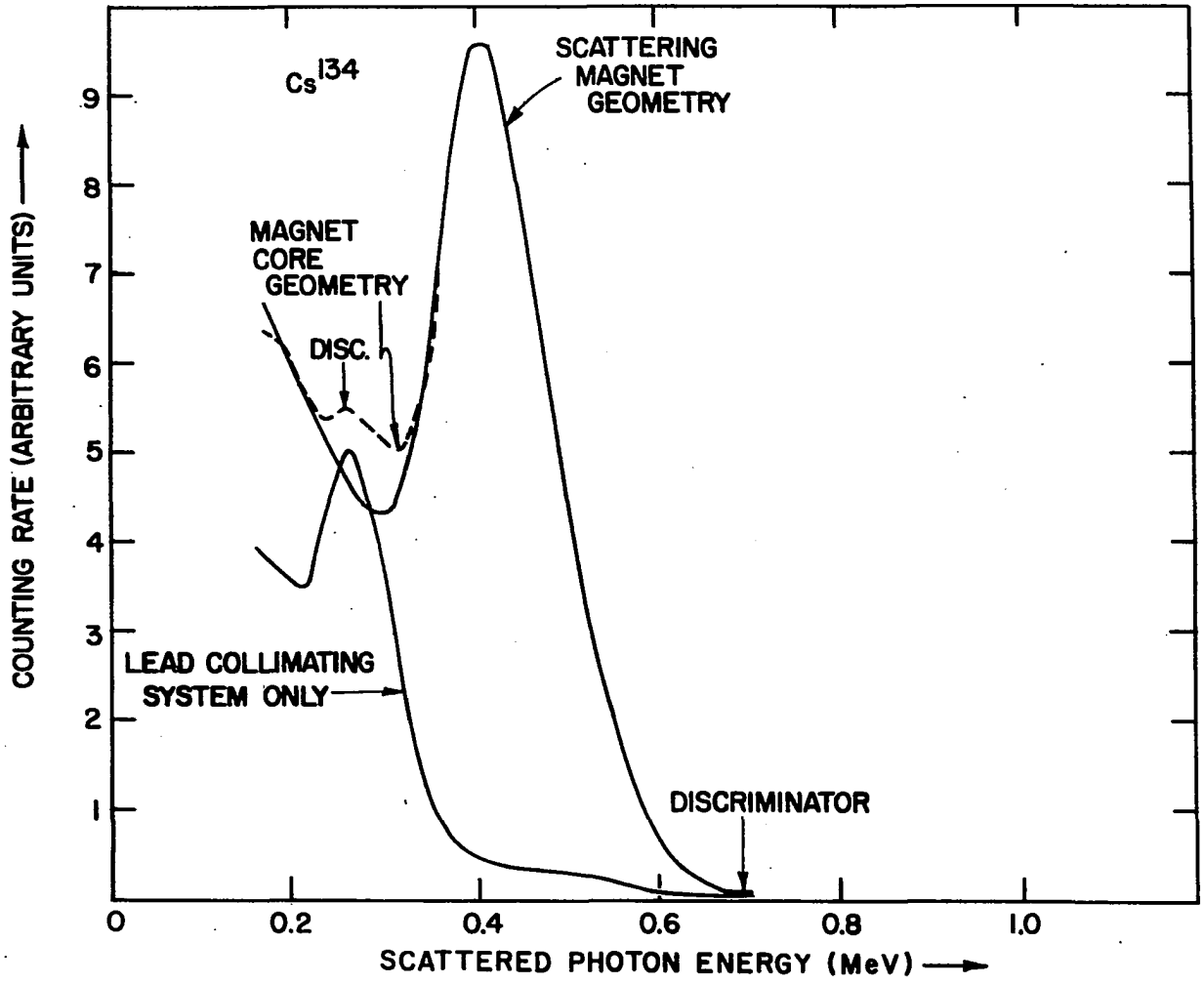
Cs 134
SCATTERING MAGNET GEOMETRY
MAGNET CORE GEOMETRY
DISC.
LEAD COLLIMATING SYSTEM ONLY
DISCRIMINATOR
COUNTING RATE (ARBITRARY UNITS)
SCATTERED PHOTON ENERGY (MeV)
0
0.2
0.4
0.6
0.8
1.0
1
2
3
4
5
6
7
8
9

Figure 6. Co^{60} gamma-ray spectra from three different geometrical arrangements used to determine nonpolarized scattering corrections

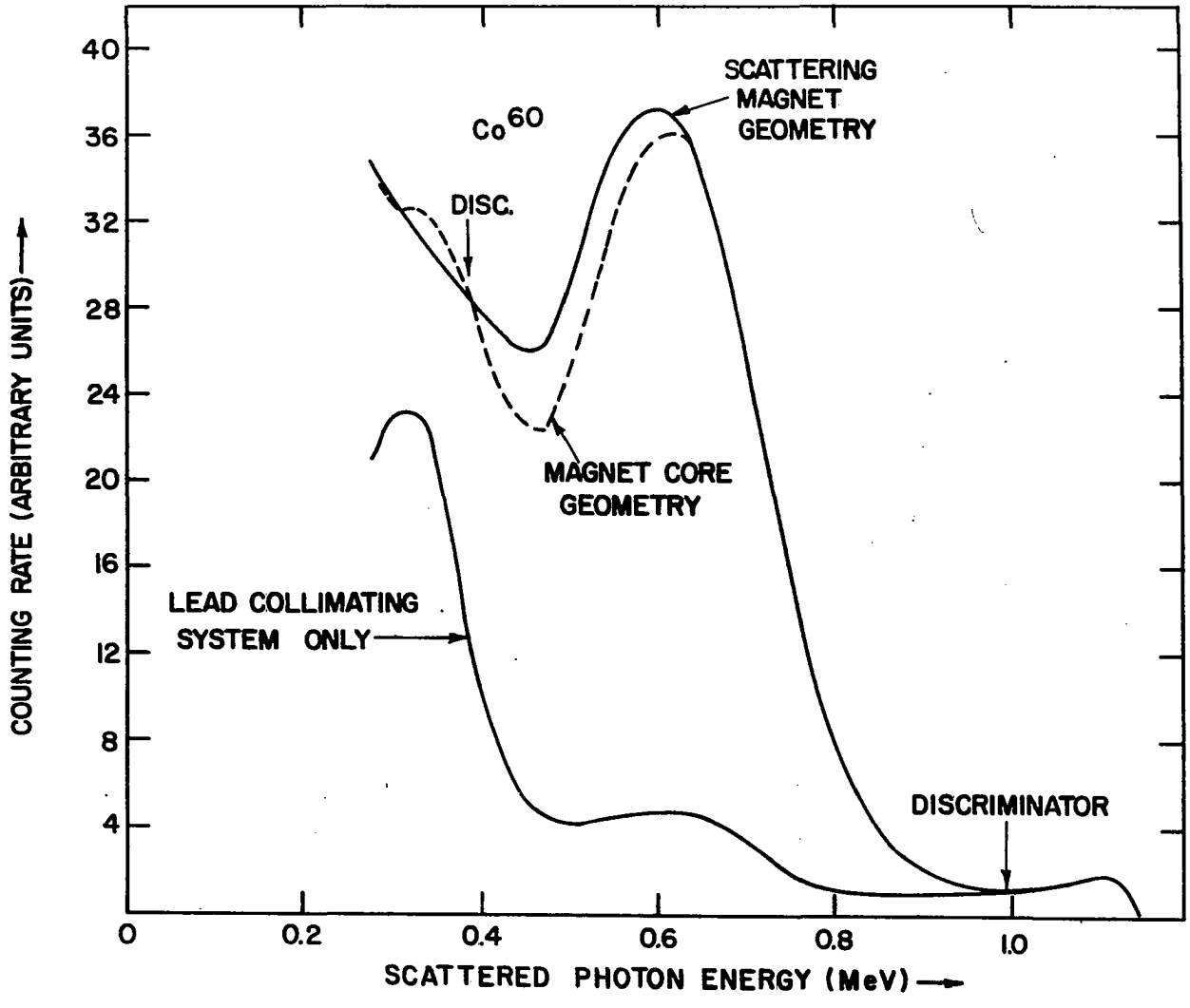
COUNTING RATE (ARBITRARY UNITS)
40
36
32
28
24
20
16
12
8
4
0
0.2
0.4
0.6
0.8
1.0
SCATTERED PHOTON ENERGY (MeV)
Co60
SCATTERING MAGNET GEOMETRY
DISC.
MAGNET CORE GEOMETRY
LEAD COLLIMATING SYSTEM ONLY
DISCRIMINATOR

Figure 7. Sb^{124} gamma-ray spectra from three different geometrical arrangements used to determine nonpolarized scattering corrections

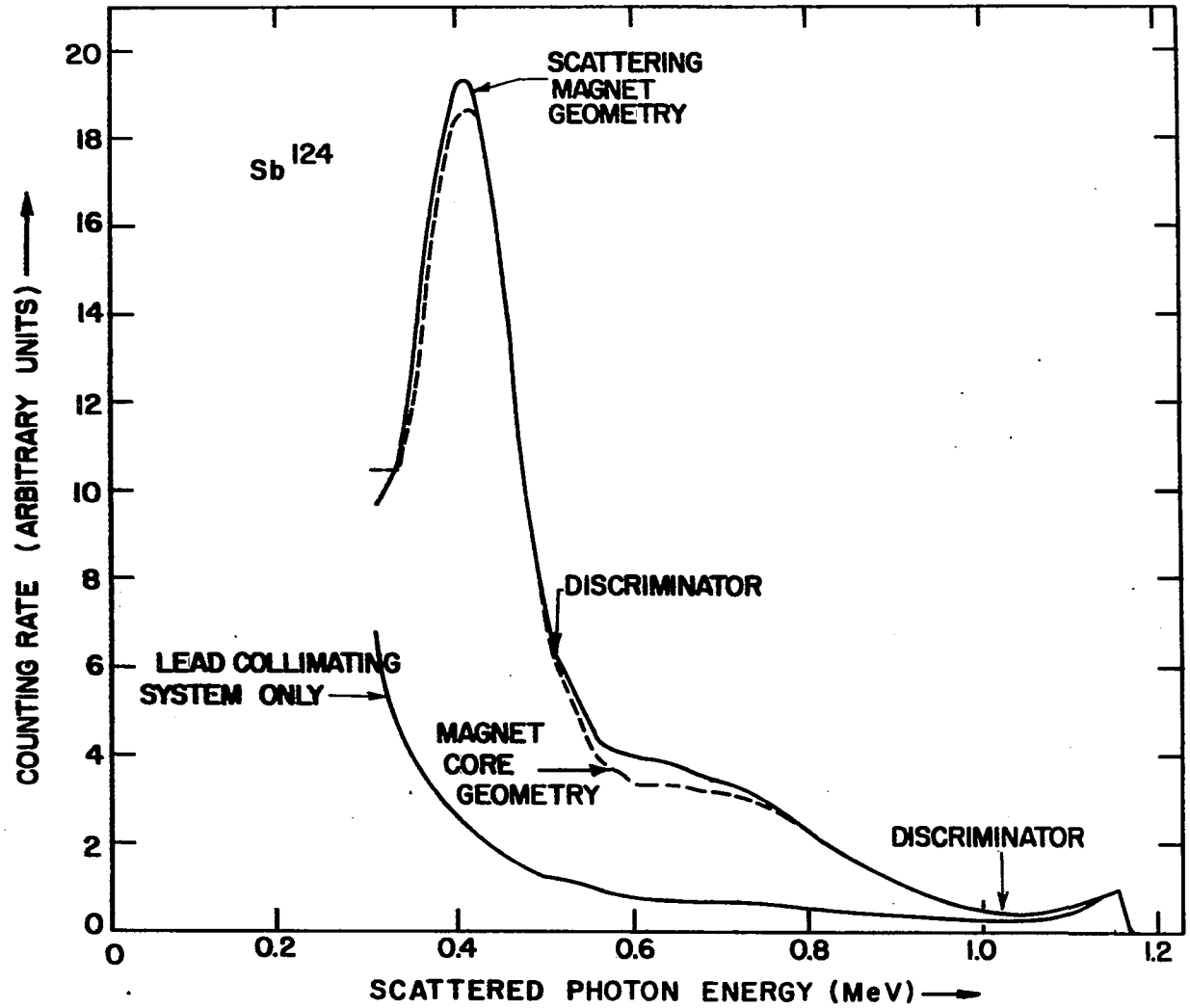
Sb 124
SCATTERING MAGNET GEOMETRY
DISCRIMINATOR
LEAD COLLIMATING SYSTEM ONLY
MAGNET CORE GEOMETRY
DISCRIMINATOR
COUNTING RATE (ARBITRARY UNITS)
SCATTERED PHOTON ENERGY (MeV)
0
2
4
6
8
10
12
14
16
18
20
0.2
0.4
0.6
0.8
1.0
1.2

support structure. Since the correction was determined by subtracting the spectra taken with these two geometries, the scattering from the support canceled out; at any rate, most of this peak was outside the discriminator windows used in the asymmetry measurements.

Coincidence spectra were used for the cesium and antimony nonpolarized scattering corrections. While a spectrum was recorded the beta counting rate was monitored. The coincidence spectrum was then normalized to the beta counting rates. The contribution to the coincidence spectra from room background was negligible.

For the Co^{60} case either the coincidence or the singles spectra could have been used since the observed gamma rays were both in coincidence with betas. The singles spectra were used because the statistical errors were less. Room background again was not a serious problem. It was found to be small and nearly the same for all three geometries. However, the room background spectrum was subtracted from the ungated spectra in determining the Co^{60} correction.

For the typical discriminator settings shown in the figures, the fractions of gamma rays scattered from nonpolarized material were 19% for Cs^{134}, 23% for Co^{60}, and 31% for Sb^{124}. The correction factors to the raw asymmetry, used in Equation 14, were respectively 1.24, 1.30, and 1.45. Although the antimony correction was somewhat larger it was found to be very insensitive to discriminator setting. Thus the antimony results were less effected by gain changes which occurred during the long raw asymmetry measurements. Tests were done on two different Co^{60} sources, one at the beginning and one at the end of the investigation. The resulting corrections differed by less than one percent.

d. Coincidences due to backscattered beta rays Effects due to the scattering of beta rays from the thin source backing and from the source material itself were thought to be small compared to the other background effects. Corrections to the raw asymmetry were difficult to determine numerically because of a lack of detailed knowledge of the thickness of sources.

Other investigators (44,45,48) have made one or two percent backscatter corrections to the raw coincidence asymmetry for sources evaporated on 1 mg/cm^2 Mylar. Since the sources used in this investigation were of reasonably uniform appearance and were deposited on the same type of very thin backing it was felt that the error in the coincidence asymmetries due to backscattering effects probably did not exceed two percent. Because the beta energy ranges involved were roughly similar (particularly in the case of Sb^{124} and Co^{60} with the same lower thresholds) the backscattering effects would be expected to cancel in the relative comparison with Co^{60} (note Equations 11 and 13). This contention is supported by the fact that saturation backscattering, i.e., from thick backings, for a given scatterer has been found to be independent of energy over the range 0.17 to 1.7 MeV (73). The resulting error in the asymmetry parameter due to backscattering effects was estimated to be less than one percent. Consequently, no correction for backscattering was included in the final results.

3. Average v/c

The average v/c was determined for each source from the portion of the theoretical beta spectrum included in the beta energy discriminator

window. The various theoretical spectral shapes were calculated from Equation 2 using the end point energies from Nuclear Data Sheets (23) and the modified Fermi functions tabulated by Rose et al. (11).

The energies of the beta pulse height discriminator levels were obtained using the K internal conversion line of Cs^{137} at 624 keV and the K conversion line of Hg^{203} at 193 keV. The centroid of the K line of mercury was determined after subtracting the contribution of the continuous beta spectrum with end point at 212 keV. The small contribution due to the L conversion lines of mercury, with average energy at 265 keV, was also subtracted. Although the centroid of the L lines could not be located as accurately as that of the K line, this point served as a rough check on the calibration.

Beta calibration sources were prepared in the same way as those under investigation, and calibration runs were taken under the same experimental conditions.

A correction was applied for the energy lost by electrons in transmission through the air and Mylar before reaching the detecting crystal. From Nelms (74) the mean energy loss for 624, 265, and 193 keV electrons was found to be 11, 14, and 16 keV respectively. The correction made almost no difference in the average v/c; however, the linearity of the extrapolation to the lower beta discriminator levels for Co^{60} and Sb^{124} at approximately 140 keV was improved slightly.

The beta discriminator was calibrated before and after each 10 day series of asymmetry determinations. An average based on daily observations of the beta counting rate was used. The gradual shift in the portion of the spectrum included in the discriminator windows was thus

adequately taken into account. (The drift in $\overline{v/c}$ was always less than 1%). The values of $\overline{v/c}$ obtained by combining all runs for each isotope are shown in Table 4.

III. ANALYSIS OF DATA

A. The Determination of Asymmetry Parameters

The method used in this investigation to measure the degree of circular polarization of gamma rays, $P_c = A\, v/c \cos\theta$, from which the asymmetry parameter A can be determined, is based upon the dependence of the Compton scattering cross section on the angle between the incident photon momentum $\underline{k}_o$ and the direction of electron spin $\underline{S}$ (see Figure 8). The intensity of scattered photons of momentum $\underline{k}$ is proportional to the Compton scattering cross section which can be written in the form (70,75)

$$d\sigma = \frac{r_o^2}{2} \left(\frac{k}{k_o}\right)^2 \left[d\sigma_o + P_l\, d\sigma_l + f\, P_c\, d\sigma_c\right],$$

where r_o is the classical electron radius, P_l is the degree of linear photon polarization, and f is the fraction of oriented electrons in the iron. The polarization independent part of the cross section $d\sigma_o$ and the polarization dependent parts, $d\sigma_l$ and $d\sigma_c$, are given by

$$d\sigma_o = 1 + \cos^2\theta + (k_o - k)(1 - \cos\theta)$$

$$d\sigma_l = \sin^2\theta$$

$$d\sigma_c = -(1 - \cos\theta)\left[(k_o + k)\cos\theta\cos\psi + k\sin\theta\sin\psi\cos\phi\right]$$

where, as shown in Figure 8, θ is the scattering angle, ψ is the angle between the direction of the incident photon $\underline{k}_o$ and the electron spin $\underline{S}$, and ϕ is the angle between the $(\underline{k}_o - \underline{S})$ plane and the $(\underline{k}_o - \underline{k})$ plane (see Figure 8a). For the orientation shown in the figure, the angle ψ is equal to the angle α made by the incident photon direction and the crystal axis.

Figure 8. Definition of geometrical quantities
(a) A Compton scattered photon
(b) A detected beta ray followed by a gamma ray Compton scattered from the magnet

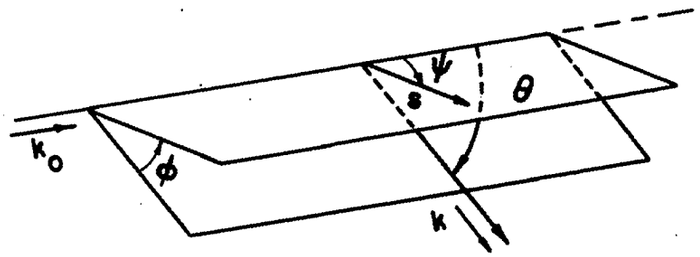
k_o
ϕ
ψ
s
θ
k

(a)

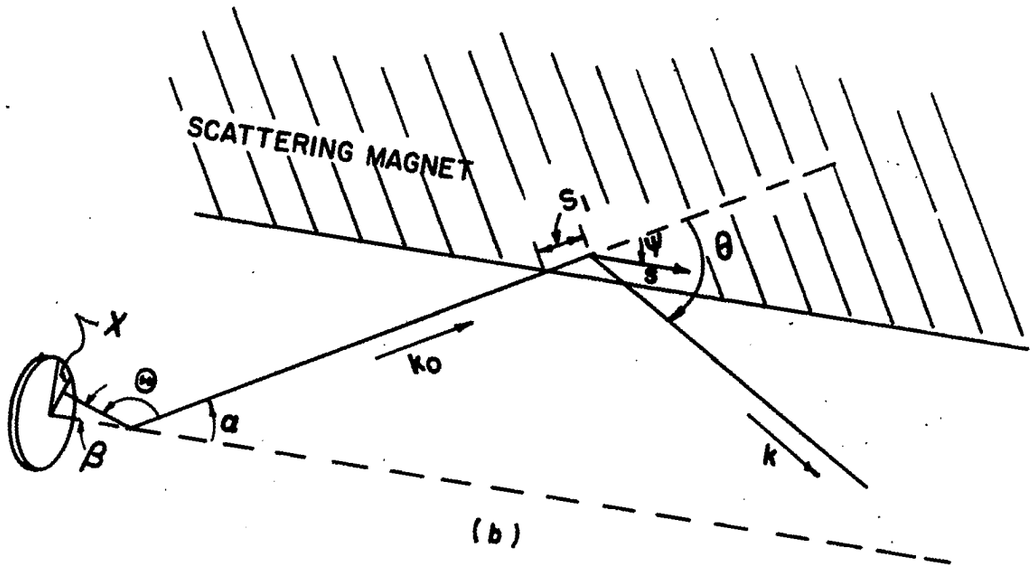
SCATTERING MAGNET
S_1
ψ
s
θ
X
ω
α
β
k_o
k

(b)

Let N refer to the observed coincidence counting rate corrected for undesired coincidences (see Chapter II) and normalized to the product of the beta and gamma singles rates. We have $N^{\pm} \propto d\sigma = d\sigma_o \pm f\ P_c\ d\sigma_c$, where the + (-) sign corresponds to the case in which electron spin and gamma momentum tend to be parallel (antiparallel). The asymmetry parameter A can be determined from the relative difference in coincidence counting rates δ which for a polarization analyzer with given angles α, β, and Θ (shown in Figure 8) has the form

$$\delta = \frac{N^- - N^+}{N^- + N^+} = \frac{f\ P_c\ d\sigma_c^-/d\sigma_o}{1 + P_1\ d\sigma_1/d\sigma_o} \approx f\ P_c\ \frac{d\sigma_c^-}{d\sigma_o} = f\ A\ v/c\ \cos\Theta\ \frac{d\sigma_c^-}{d\sigma_o} \qquad (7)$$

Here, P_1 was assumed to be negligible*(29). In practice v/c must be averaged over the part of the beta spectrum accepted by the beta discriminator window. The factor $\cos\Theta\ d\sigma_c^-/d\sigma_o$ must be calculated for each incident photon energy from an average over the finite size of the beta detecting crystal, the gamma detecting crystal, and the spread of the acceptance angle α (over the volume of the scattering region).

For a given α, the angle Θ varies over the surface of the beta crystal. By integrating over angles χ and β shown in Figure 8b, the average $\cos\Theta$ can be determined. Letting $\Theta_o = \Theta + \beta$ and β_m be the maximum value of β, we have

---

*For $\Theta = 56^o$ and 1.25 MeV photons, $d\sigma_1/d\sigma_o = 0.37$. Using forward scattering Wheatley et al. (37) measured the circular polarization of photons from oriented cobalt nuclei. Their calculations of P_1 indicate effects due to plane polarization to be less than 4%. Thus, such effects are thought to be negligible here.

$$\overline{\cos\theta} = \frac{\int_0^{\beta_m}\int_0^{2\pi} \cos\theta \, d\beta \, d\chi}{\int_0^{\beta_m}\int_0^{2\pi} d\beta \, d\chi}$$

where

$$\cos\theta = \cos\theta_o \cos\beta + \sin\theta_o \sin\beta \cos\chi$$

from which

$$\overline{\cos\theta} = \cos\theta_o \frac{\sin\beta_m}{\beta_m} = -\cos\alpha \frac{\sin\beta_m}{\beta_m} \; .^{*}$$

Substitution in Equation 7 gives

$$\delta = f A \bar{v}/c \, E_{1,2}(k_o) \frac{\sin\beta_m}{\beta_m} \tag{8}$$

where the polarization analyzer efficiency $E_{1,2}(k_o)$ is defined by

$$E_{1,2}(k_o) = M E_1(k_o). \tag{9}$$

This is just the polarization analyzer efficiency for singly-scattered photons

$$E_1(k_o) = \left\langle \frac{d\sigma_c^+}{d\sigma_o} \cos\alpha \right\rangle$$

times the factor M included to correct $E_1(k_o)$ for the presence of doubly-scattered photons. An average over the NaI crystal and over the region of polarized electrons is indicated for E_1.

---

*A point source was assumed. The effect of finite source size is to increase β_m slightly (70).

For determining the asymmetry parameter A(X) of the isotope X in a comparison measurement with Co^{60} as a standard, the following definitions were convenient. Let the relative polarization response function C_{pe} be given by

$$C_{pe}(X) = \frac{E_{1,2}(Co)}{E_{1,2}(X)} \quad . \tag{10}$$

Let the relative asymmetry parameter $A_r(X)$ be defined by

$$A_r = \delta(X) \quad \frac{E_{1,2}(Co)}{E_{1,2}(X)} \quad (\bar{v}/c)^{-1} = \delta(X)\, C_{pe}(X) \quad (\bar{v}/c)^{-1} . \tag{11}$$

We then have from Equation 8

$$A(X) \propto \frac{\beta_m}{f \sin \beta_m} \quad A_r(X).$$

Keeping β_m and f constant for all sources and assuming that the asymmetry parameter for Co^{60} has the theoretical value A = -1/3, we have

$$A(X) = -\frac{1}{3} \quad \frac{A_r(X)}{A_r(Co)} . \tag{12}$$

Note that the comparison measurement does not depend on a knowledge of the fraction of polarized electrons f (which is not trivial to determine), nor is it necessary to know β_m if the beta crystal to source distance remains fixed. Furthermore the calculation of the magnet response as a function of incident photon energy need only be a relative one, which tends to be more accurate than an absolute calculation.

In the computation of the raw coincidence asymmetry the coincidence counting rates were normalized to the product of the beta and gamma singles counting rates. This reduced systematic effects such as possible slight differences in counting time for the two magnet orientations or systematic gain differences due to the influence of the stray magnetic field on the phototubes.

The raw asymmetry R was corrected for background coincidences N_b for which the asymmetry was zero. With N_t the total coincidence counting rate and R defined by

$$R = \frac{N_t^- - N_t^+}{N_t^- + N_t^+},$$

we have

$$\delta = \frac{N^- - N^+}{N^- + N^+} = \frac{N_t^- - N_t^+}{N_t^- + N_t^+ - 2N_b} = R \frac{1}{1 - \frac{2N_b}{N_t^- + N_t^+}} = \frac{R}{1-f_b}, \quad (13)$$

where f_b is the fraction of the total coincidence counting rate due to the background counting rate. It was assumed in Equation 13 that the same background counting rate was measured for both orientations of the magnet. Such an assumption is valid since the observed difference in total coincidence counting rates was less than 1% in all cases. The background correction to the raw asymmetry is given by

$$\frac{1}{1 - f_b} = \left[\frac{1}{1 - f_{rc}}\right] \left[\frac{1}{1 - f_{\gamma\gamma}}\right] \left[\frac{1}{1 - f_{np}}\right], \quad (14)$$

where f_{rc}, $f_{\gamma\gamma}$, and f_{np} refer to the fraction of the total coincidences due respectively to random coincidences, gamma-gamma coincidences, and coincidences due to gamma rays reaching the crystal without scattering from the region of polarized electrons. The experimental determination of these quantities has been discussed in Chapter II.

Coincidences due to room background were negligible. From the discussion of Section E, Chapter II, no correction to the raw asymmetry was thought needed for the small backscattered beta-ray contribution. This completes the information needed to determine asymmetry parameters except for the calculation of the polarization detection of the analyzer magnet which will be now discussed.

B. The Calculation of the Response of the Circular Polarization Analyzer

1. Single Compton scattering

A detailed calculation of the magnet polarization detection efficiency $E_{1,2}(k_o)$ as a function of incident photon energy would require elaborate Monte Carlo procedures. An approximate method according to Schopper (70) was used involving graphical integration over the geometry. This was estimated to be good within 3%.

The single Compton scattering response is given by

$$E_1(k_o) = \left\langle \frac{d\sigma_c^+}{d\sigma_o} \cos\alpha \right\rangle = \frac{\int \langle \overline{\epsilon(\alpha)}\, d\sigma_c^+ \omega_p \rangle \frac{\sin\alpha}{\sigma_{t_1} + g\,\sigma_{t_2}} \cos\alpha\, d\alpha}{\int \langle \overline{\epsilon(\alpha)}\, d\sigma_o \rangle \frac{\sin\alpha}{\sigma_{t_1} + g\,\sigma_{t_2}}\, d\alpha} . \tag{15}$$

The average inside the integrals represented by brackets means an average over the path length S_1 in the magnet for a particular angle α. (see Figure 8b). Here $\overline{\epsilon(\alpha)}$ is the average relative probability of detection for a scattered photon resulting from a photon incident at the angle α, σ_{t_1} and σ_{t_2} are the total polarization independent absorption cross sections in barns/atom for the incident and scattered photons; and $g = S_1/S_2$, where S_2 is the photon path length in the iron after scattering. The factor $(\sigma_{t_1} + g\,\sigma_{t_2})^{-1}$ expresses the dependence of the number of detected photons on the probability of absorption in the iron. The factor was derived assuming that photon transmission through the region of partially polarized electrons was negligible, a good assumption for the case of the 1" thick scattering magnet used in this investigation.

The factor ω_p, appearing only in the numerator, takes into account the polarization dependent absorption of photons in the iron. The factor was computed from

$$\omega_p(\alpha) = 1 + \frac{\langle d\sigma_o \rangle}{\langle d\sigma_c \rangle} \quad \frac{\sigma_{c_1} \cos\alpha + g\ \chi'\ \sigma_{c_2} \cos(\theta - \alpha)}{\sigma_{t_1} + g\,\sigma_{t_2}} \quad ,$$

where σ_{c_1} and σ_{c_2} are the total polarization dependent cross sections for the incident and scattered photons and have the form (76, p. 180)

$$\sigma_c(k') \propto (\underline{k}' \cdot \underline{S}) \left[\frac{1 + 4k' + 5k'^2}{k'(1 + 2k')^2} - \frac{1 + k'}{2k'^2} \operatorname{Ln}(1 + 2k') \right] \quad ;$$

$$(k' = k_o \text{ or } k).$$

The factor χ' is the ratio between the photon polarization before and

after scattering. This was computed for each scattering site and each incident photon energy from (75,76 p. 189)

$$\chi' = \frac{2\cos\phi + k_o^2 (1 - \cos\phi)^2 \cos\phi}{1 + \cos^2\phi + k_o^2 (1 - \cos\phi)^2}$$

$E_1(k_o)$ was calculated for values of incident photon energy 1.69, 1.25, and 0.7 MeV corresponding to the transitions of Sb^{124}, Co^{60}, and Cs^{134}, respectively. The last two were averages of two gamma rays both in coincidence with betas (1.332 and 1.173 MeV for Co^{60}; 0.796 and 0.605 MeV for Cs^{134}).

The assumption of a point source for these calculations was justified by the small size of the source compared to the dimensions of the magnet.

A preliminary calculation revealed that the quantities in the integrals varied smoothly with α over the length of the magnet. It was thus sufficient to perform the detailed calculation for seven discrete angles across the entrance aperture. For each angle the quantities in the integrands were computed for two path lengths into the magnet, one shallow and one deep. A weighted average of the two was taken based on a determination of the relative probability of detection as a function of penetration depth into the magnet. The probability of transmission to the depth S_1 and the probability of transmission along the exit path S_2 were taken into account. The absorption cross sections of Davisson and Evans (77) were used, and exit paths to the center of the available detection volume of the NaI crystal were assumed. The average penetration depth for k_o = 1.69 MeV was found to be 8.1 mm for the maximum entrance angle, 9.3 mm for the middle case, and 8.9 mm for the minimum α. For k_o = 1.25 MeV,

$\langle S_1 \rangle$ = 8.2 mm for the middle α; and for k_o = 0.7 MeV, $\langle S_1 \rangle$ = 7.2 mm. Thus the photons detected by the crystal were predominately scattered from sites near the surface of the magnet even in the case of the most penetrating gamma ray studied.

Computing the average of the factors in the integrals over the NaI crystal was complicated by the dependence of the detection efficiency on the scattered photon energy which varied considerably over the crystal; e.g., for the case $\alpha = 23^\circ$, S_1 = 9 mm, and k_o = 1.69 MeV, the scattered photon energy varied from 920 keV to 560 keV across the crystal. The situation was also complicated by the rapid change in path lengths through the lateral surface of the cylindrical crystal as the photon entrance parameters were varied.

The following procedure for averaging quantities over the crystal was, however, found to be adequate. For a given scattering site (α, S_1) in the magnet, a certain volume of the crystal was defined by the lead aperture for detection of scattered photons. The circular aperture was divided into 14 different regions of about equal area. The relative total detection efficiency ϵ_T was calculated for a central gamma ray in each region, where ϵ_T is the relative probability that the scattered gamma ray interacts with the crystal producing any pulse contributing to the total spectrum. In this case $\epsilon_T = \epsilon_i \, d\Omega$, where $d\Omega$ is the solid angle subtended at the scattering point by an aperture area element, and ϵ_i is the average intrinsic efficiency of detection for photons passing through the element. This was approximated by $\epsilon_i = 1 - e^{-\tau(k) L}$, the intrinsic efficiency of the central ray, where L is the path length through the crystal, and $\tau(k)$ is the total interaction cross section excluding coherent scattering for

the central photon with energy k (78). The relative detection probability for photons from a given scattering site was just the sum of the contributions from each of the elements in the aperture.

The requirement that scattered photon energies exceed the lower discriminator level was taken into account in the determination of the relative detection efficiency. This consideration was significant only in the case of k_o = 1.69 MeV. Here, the relatively high discriminator level at 515 keV imposed a maximum scattering angle of about 72^o. The reduced NaI volume available for detection, resulting in a decrease in the detection efficiency, was appropriately taken into account in the calculation.

The calculation of the relative detection efficiency was tested with a Cs^{137} point source emitting 662 keV photons. The magnet was removed and spectra from the NaI crystal were taken with this source placed at each of the scattering sites used for the calculation. The results obtained by integrating these spectra and plotting the total counting rate as a function of the angle α were in reasonably good agreement with the calculated relative detection probability. Even better agreement could probably have been obtained by a finer division of the aperture grid; however, only an approximate knowledge of the efficiency was needed as will be shown later.

In addition, these spectra yielded for each scattering site the ratio of the counts detected in the photo peak to the counts detected in the total spectrum for 662 keV photons. The peak-to-total ratio was found to increase gradually with increasing α; i.e., P/T increased as the scattered photons entered the crystal face at less acute angles. The values obtained with this off-axis geometry were intermediate between the peak-to-total

ratios obtained by Vegors et al. (78) for 1.75" dia. x 2" thick and for 3" dia. x 3" thick crystals with the source on the crystal axis. The peak-to-total ratio for scattered photons was thus estimated by using the results of Vegors et al. (78, pp. 81-83).

The relative detection probability $\epsilon(\alpha) = \epsilon_T P/T$ was calculated for each k_o and each scattering site using the above mentioned estimates of the peak-to-total ratio. The relative total detection efficiencies ϵ_T were here determined by replacing the cross section for the 662 keV photon with cross sections for each of the 14 representative scattered photons.

The quantities other than $\epsilon(k_o, \alpha)$ in the integrands of Equation 15, i.e., $d\sigma_c$, $d\sigma_o$, ω_p, and $(\sigma_{t_1} + g\,\sigma_{t_2})^{-1}$ were averaged over the NaI crystal by dividing the crystal into three different regions. In region one the average scattering angle was smallest, the scattered photon energy was largest, and the average intrinsic efficiency was greatest since the path lengths through the crystal were longer. In the third region most of the photons were directed out through the lateral surface of the crystal making the intrinsic efficiency considerably less. The second region represented conditions intermediate between the two. The desired quantities were computed for the median photon energy associated with each region. The average over the crystal for a particular scattering site was found by weighting each of the 3 regions according to its estimated detection efficiency. The integrals were then evaluated by graphical integration of the angle α over the entrance aperture.

The results of the calculation of the polarization efficiency for singly-Compton scattered photons are given in Table 2.

Table 2. Calculated magnet polarization detection efficiencies for singly-Compton scattered photons

k_o(MeV)	$E_1(k_o)$	$\frac{E_1(1.25)}{E_1(k_o)}$
0.7	0.365	1.177
1.25	0.430	1.000
1.69	0.444	0.967

The sensitivity of the calculated response to the weighting factor $\frac{\epsilon(\alpha)}{\sigma_1 + g\,\sigma_2}$ which appears in both the numerator and denominator of Equation 15 was tested for k_o = 1.69 MeV by setting the factor equal to one for all α. The result, $E_1(1.69) = 0.438$, differed from the value used for calculating asymmetry parameters (and shown in the table), by only 1.4%. This was an indication that the estimated relative detection efficiency did not have to be accurately known.

The calculation was also not very sensitive to the method used in averaging over the NaI crystal. The value $E_1(1.69) = 0.454$ was obtained by considering only region one in the crystal (1/3 of the crystal volume corresponding to small scattering angles). This result is within 2.3% of the value shown in the table.

The calculation of magnet polarization detection efficiencies for Sb^{124} and Cs^{134} in a relative comparison with Co^{60} would be expected to be less sensitive to the assumptions and procedures used than would be an absolute efficiency calculation. The relative efficiencies computed

for the case of single Compton scattering were thought to be fairly reliable. The influence of higher order processes, however, was much more difficult to determine exactly.

2. Plural scattering

The effect of higher order scattering processes on the magnet polarization detection efficiency has been discussed by Schopper (70) and investigated experimentally by Huber et al. (79). The intensity of photons reaching the crystal after having undergone three or more collisions was thought to be negligible, the mean free path of 1 MeV photons in iron being on the order of 1 cm. The intensity of doubly-scattered photons, however, was expected to be significant. This was found to be the case from an estimate of the ratio $\rho(\alpha)$ of the intensity of doubly-scattered to singly-scattered photons.

The integral expression derived by Schopper (70, p. 172) for this ratio was evaluated for the scattering magnet used in this investigation. The factor $M(\alpha)$ by which the calculated single scattering polarization response must be reduced was determined from

$$M(\alpha) = \frac{1 + \rho m}{1 + \rho} \tag{16}$$

and

$$m(\alpha) = \frac{\left\langle \frac{d\sigma_c(\theta_1)}{d\sigma_o(\theta_1)} \right\rangle + \chi_1 \left\langle \frac{d\sigma_c(\theta_2)}{d\sigma_o(\theta_2)} \right\rangle}{\left\langle \frac{d\sigma_c(\theta)}{d\sigma_o(\theta)} \right\rangle}, \tag{17}$$

where θ is the single scattering angle, θ_1 (θ_2) is the first (second) scattering angle of the double scattering, and χ_1 is the change in polar-

ization of the doubly-scattered photon as the result of the first interaction. In the calculation of $\rho(\alpha)$ and $m(\alpha)$ it was assumed that $\theta_1 + \theta_2 \approx \theta$, which represents a condition appropriate for the detection of the doubly-scattered photon. The results for a typical scattering site are shown in Figure 9. $m(\alpha)$ and $\rho(\alpha)$ were found by averaging the functions, $m(\theta_1)$ and $\rho(\theta_1)$ for this particular scattering site over the first scattering angle from $\theta_1 = 0$ to $\theta_1 = \theta$. The values of m are seen to approach one as the first scattering angle θ_1 approaches zero and also as θ_1 approaches θ. The factor M thus differs from unity mainly due to photons scattering twice through angles approximately half that of the single scattering angle; in this case the intensity of doubly-scattered photons was maximum as was the deviation of m from one.

The results obtained for the correction factor averaged over the magnet geometry are shown in Table 3 along with the average intensity ratio $\langle \rho(\alpha) \rangle$. Despite the significant percentage of doubly-scattered events the correction to the magnet response was not severe.

Table 3. Results of the polarization detection efficiency calculation including corrections for double scattered photons

k_o(MeV)	$\langle \rho(\alpha) \rangle$	$\langle M \rangle$	$\langle M(2\rho) \rangle$	$\frac{\langle M(k_o) \rangle}{\langle M(1.25) \rangle}$	C_{pe}
0.7	0.13	0.974	0.953	0.985	1.195
1.25	0.15	0.989	0.981	1.000	1.000
1.69	0.18	0.998	0.996	1.010	0.958

Figure 9. Dependence of the factors in Equation 16 on the first scattering angle θ_1 of the double scattering.

(a) $m(\theta_1)$, the factor defined by Equation 17

(b) $\rho(\theta_1)$, the intensity ratio of doubly-scattered to singly-scattered photons

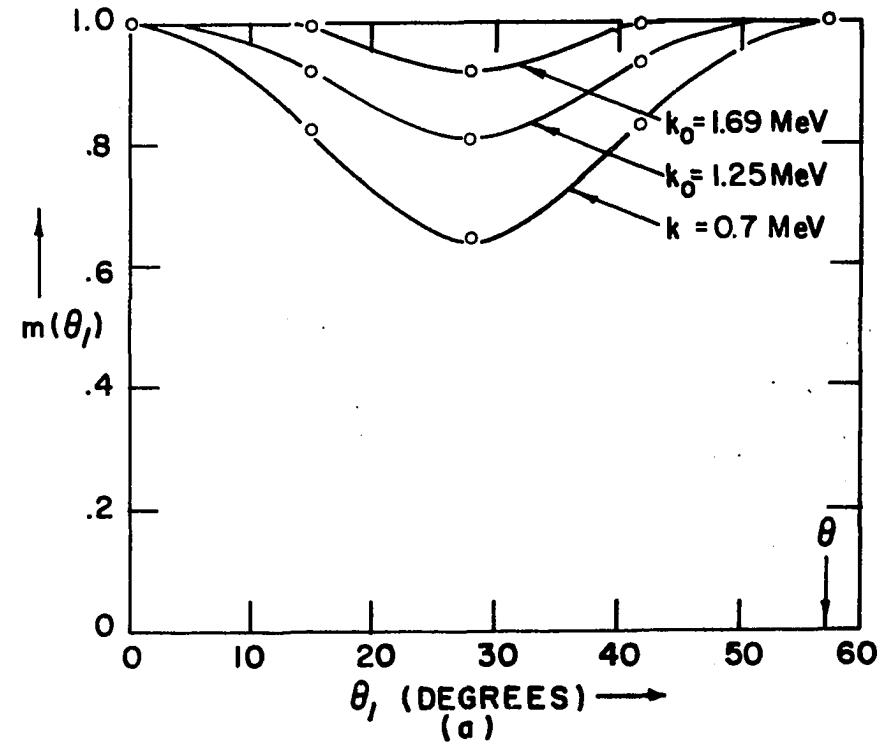
1.0
.8
.6
.4
.2
0
m(θ_l)
k_0 = 1.69 MeV
k_0 = 1.25 MeV
k = 0.7 MeV
θ
0
10
20
30
40
50
60
θ_l (DEGREES) ⟶
(a)

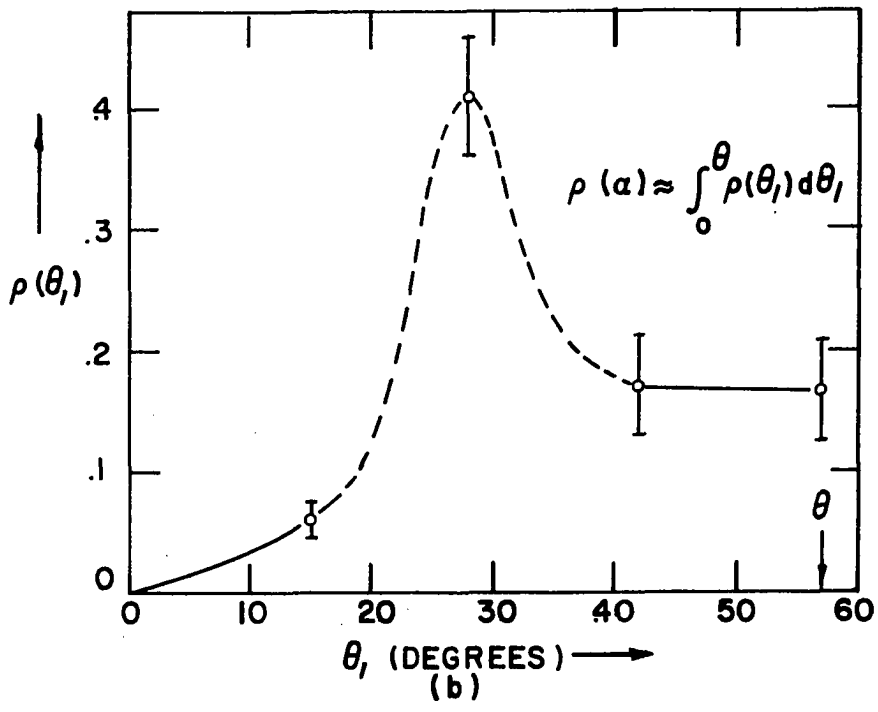
4
.3
.2
.1
0
ρ(θ_l)
ρ(α) ≈ ∫_0^θ ρ(θ_l) dθ_l
θ
0
10
20
30
40
50
60
θ_l (DEGREES) ⟶
(b)

Although m could be calculated reliably some rather crude approximations were necessary to determine $\rho(\alpha)$ from a very difficult integral expression. Consequently the factor $M(2\rho)$ is included to show the effect of doubling the above estimates of ρ. The relative polarization response function C_{pe}, (defined by Equations 9 and 10) which was used for the determination of asymmetry parameters, is also included in the table.

Huber et al. investigated the effect of multiple scattering on the polarization efficiency for Compton scattering using a similar scattering geometry and external bremmstrahlung as a source of polarized photons. Their measured polarization efficiencies were 7% ± 3% less than efficiencies calculated for singly-scattered photons $E_1(k_o)$. However this difference was independent of energy k_o for the range 600 to 1220 keV within their experimental error. If such results were applied to this geometry (requiring an extrapolation in the case of Sb^{124}), there would be no correction for double scattering in the relative comparison of Cs^{134} and Sb^{124} with Co^{60}. However, this was not done. Rather the estimated correction factors $\langle M(\rho) \rangle$ in the table were thought to represent the true situation more closely and were therefore used in the final computation of C_{pe}.

IV. EXPERIMENTAL RESULTS AND DISCUSSION

A. Asymmetry Parameters

The relative asymmetry parameter A_r was computed for each series of runs using Equation 11. The combined averages A_r for Co^{60}, Sb^{124}, and Cs^{134} were obtained by weighting each series with a factor (80) proportional to $[\sigma (A_r)]^{-2}$. These results are shown in Table 4 along with the weighted averages of the other significant quantities.

Table 4. Summary of experimental results

	Co^{60}	Cs^{134}	Sb^{124}
R(%)	0.419 ± 0.016	0.110 ± 0.024	-0.496 ± 0.036[a]
R[b](%)	0.010 ± 0.038	- - - - - - -	- - - - - - -
f_{rc}	0.12	0.11	0.07
$f_{\gamma\gamma}$	0.03	0.10	0.06
f_{np}	0.23	0.19	0.31
δ(%)	0.642	0.169	-0.825[a]
C_{pe}	1.00	1.20	0.96
$\bar{v}/c$	0.67	0.80	0.72
A_r	0.958 ± 0.037	0.253 ± 0.054	-1.100 ± 0.085[a]
A	-1/3	-0.088 ± 0.019	0.407 ± 0.030[c]

[a]Includes transitions other than that corresponding to the 1.69 MeV gamma ray.

[b]Compensation coil and scattering magnet currents not reversed.

[c]Corrected for transitions other than that corresponding to the 1.69 MeV gamma ray.

The raw asymmetry R^b, shown in the table, was measured under the same experimental conditions as the other cobalt runs except that the currents in the compensation coils and scattering magnet were not reversed. This result indicates stability of the apparatus.

The main contribution to each of the standard deviations $\sigma(A_r)$ was the statistical error $\sigma(R)$ in the raw coincidence asymmetry. This is given to a good approximation by $\sigma(R) = (N^- + N^+)^{-\frac{1}{2}}$. Errors of 2%, 3%, and 3% in the determination of $\overline{v/c}$, C_{pe}, and f_{np}, respectively, were included. These last errors were estimated partly from the variation in the factors which occurred during the coincidence asymmetry measurements.

The asymmetry parameters for cesium and antimony were obtained using Equation 12 in which the theoretical value for Co^{60}, $A = -1/3$, was assumed. The error in determining the relative asymmetry parameter of cobalt was included in the calculation for the standard deviations $\sigma(A)$. This contribution to $\sigma(A)$ for cesium and antimony was found to be very small.

In order to obtain the asymmetry parameter for the 1.69 MeV gamma ray emitted subsequent to the decay of the 0.621 MeV beta branch of Sb^{124}, it was necessary to make a small correction to the observed coincidence asymmetry due to the presence of undesired transitions. The decay scheme of Nuclear Data Sheets (23) shown in Figure 10 was assumed. The additional 1.66 MeV beta branch with 1.5% intensity, not important for this analysis, was suggested by Everling. (Everling, F., Dept. of Physics, Iowa State University, Ames, Iowa. Sb^{124} decay scheme. Private communication. 1964).

The observed coincidence asymmetry was the average of the asymmetries of the transitions weighted by the fraction of total coincidences f_i due to the ith transition (75). We thus have

Figure 10. Decay scheme of Sb^{124}

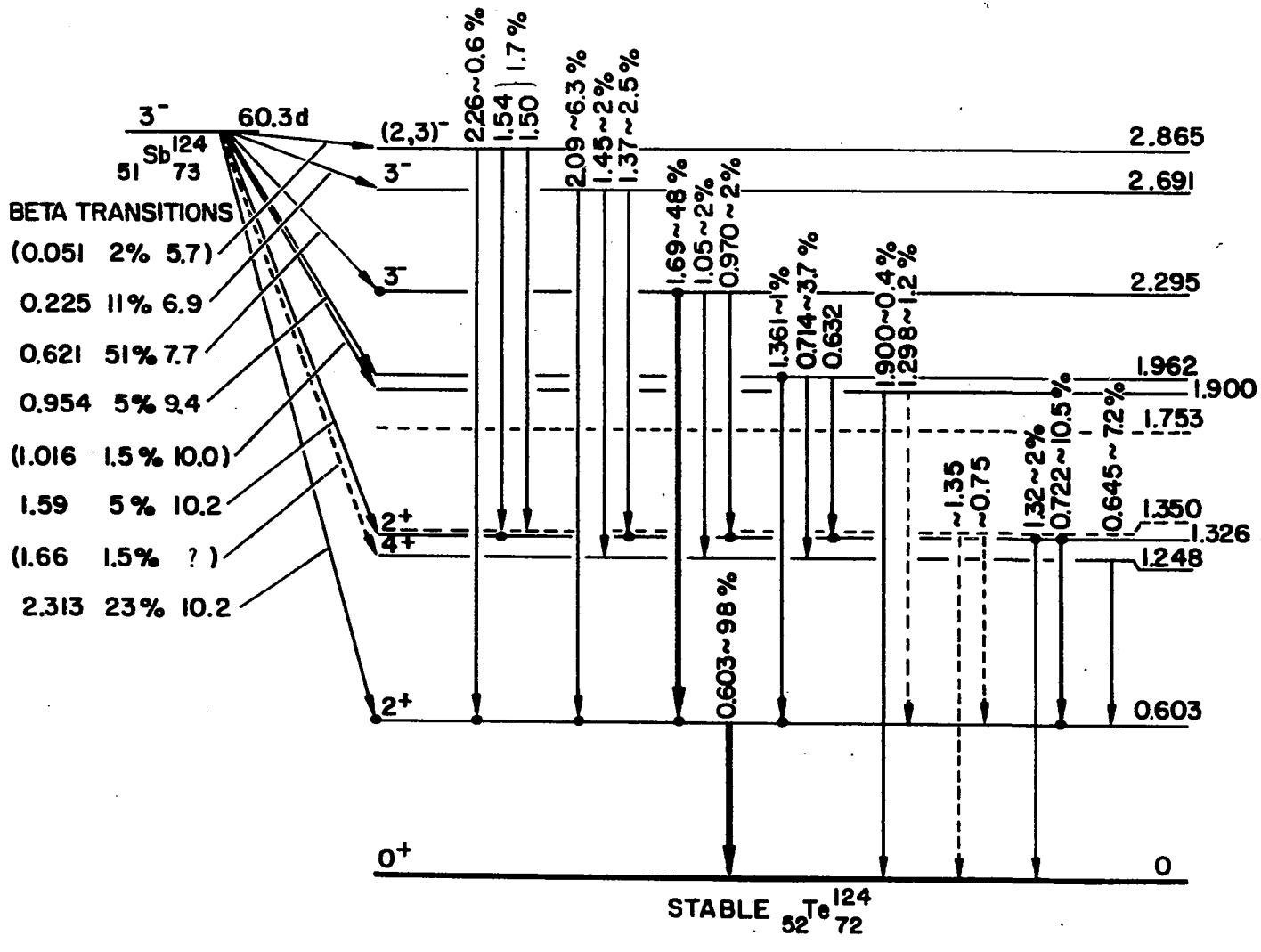
3⁻
60.3d
51 Sb 124 73
BETA TRANSITIONS
(0.051 2% 5.7)
0.225 11% 6.9
0.621 51% 7.7
0.954 5% 9.4
(1.016 1.5% 10.0)
1.59 5% 10.2
(1.66 1.5% ?)
2.313 23% 10.2
(2,3)⁻
3⁻
3⁻
2⁺
4⁺
2⁺
0⁺
2.26~0.6%
1.54 1.7%
1.50
2.09~6.3%
1.45~2%
1.37~2.5%
1.69~48%
1.05~2%
0.970~2%
1.361~1%
0.714~3.7%
0.632
1.900~0.4%
1.298~1.2%
~1.35
~0.75
1.32~2%
0.722~10.5%
0.645~7.2%
0.603~98%
2.865
2.691
2.295
1.962
1.900
1.753
1.350
1.326
1.248
0.603
0
STABLE 52 Te 124 72

$$\overline{\delta} \propto \sum_i f_i A_i \overline{v}/c_i \left(C_{pe_i}\right)^{-1} \qquad (18)$$

The relative coincidence intensities f_i were proportional to the product of the beta and gamma singles intensities. Therefore the relative beta singles intensities were estimated using the branching ratios from the decay scheme and integrating the theoretical beta spectrum for each branch between the limits determined by the beta discriminator. The relative intensities of the various gamma rays were calculated by applying the following equation to each photon energy (79):

$$N(k) = \int \frac{\epsilon(k,\alpha)\, d\sigma(k)}{\sigma_1 + g\,\sigma_2} \sin\alpha\, d\alpha \quad ,$$

where N(k) is the intensity of scattered photons detected by the NaI crystal.

The relative detection probability $\epsilon(k,\alpha)$ was obtained for each k in the manner described in Chapter III, Section B. It was found that approximately 89% of the total coincidence rate was due to the transition of interest. Thus, it was not necessary to calculate the coincidence intensities due to other transitions very accurately. It was sufficient to use allowed spectral shapes for all beta transitions in order to calculate the average v/c for each branch. The factor C_{pe} was determined by interpolating between values obtained for photon energies 0.7, 1.25, and 1.69 MeV.

Using the expressions derived by Morita (39) for circularly polarized gamma rays in triple cascade transitions it was found that the A_i's for the allowed contaminants in the antimony decay differed from the asym-

metry parameter for the main transition A_1 only by numerical factors. The determination of these numerical factors yielded the remaining information needed to correct Equation 18 for the presence of other allowed transitions.

The small contribution of the 1.59 MeV beta → 1.32 MeV gamma first-forbidden transition (< 1%) to the measured asymmetry was estimated using the experimental results of Alexander and Steffen (81) on the 2.31 MeV first-forbidden beta transition. The theoretical expressions of Kotani and Ross (82) were also used. The extension of the experimental results to the 1.59 MeV beta transition was thought possible because of the similarity in gamma multipolarities and beta ft values.

The remaining coincidence counting rate, approximately 4%, was due to transitions from levels with unknown spin states. The value of A_1 shown in Table 4 was determined from the measured asymmetry assuming that the unknown transitions were first-forbidden as was suggested by their ft values. The magnitude of A_1 would not be significantly altered if this assumption were not valid.

No corrections for competing transitions were needed for Cs^{134} and Co^{60}. With the beta discriminator levels used, a negligible fraction of total coincidences was due to the undesired 410-keV branch in the case of cesium. There were no competing transitions in the case of cobalt.

B. Matrix Element Ratios

The theoretical relation between the asymmetry parameter A and the matrix element ratios $Y = \frac{C_V M_F}{C_A M_{GT}}$ was derived from the expressions of Morita (39) for the cases of Cs^{134} and Sb^{124}. The results are shown in

Figures 11 and 12. The theoretical curve was computed assuming the (V-A) beta-decay interaction and time reversal invariance. These assumptions are summarized in Equation 5. Each of the transitions of interest are shown in the figures including the spins and parities used in calculating the theoretical curves.

For these allowed transitions with $j_i = j_f$, the theoretical relation between A and Y is of the form

$$A = \frac{a\,Y + b}{1 + Y^2},$$

where a and b are parameters depending on the spins of the initial and final nuclear states and the multipole order of the gamma rays. The percentage admixture of higher gamma-ray multipoles was taken to be zero in both cases since the 1.69 MeV gamma ray emitted in the decay of antimony was nearly pure electric dipole, and both gamma rays of cesium were nearly pure electric quadrupole (23). In addition the theoretical curve, according to Morita, should be the same for both gamma rays of interest for cesium.

A small value of the Fermi matrix element M_F is predicted by the isotopic spin selection rule (48). Consequently, for each nuclide the smaller of the two values of Y which could be obtained from the double-valued theoretical relation and the measured value of A was assumed to be the correct one. This value of Y is plotted in each of the figures. Though not rigorous because of charge dependent (and perhaps meson exchange) effects in the nucleus, the isotopic spin selection rule requires that the Fermi component be small compared to the Gamow-Teller contribution, and consequently that Y be small.

Figure 11. Experimental results for A, the asymmetry parameter, in the case of Cs^{134}. The curve is the theoretical relation between A and Y calculated assuming the (V-A) beta decay interaction

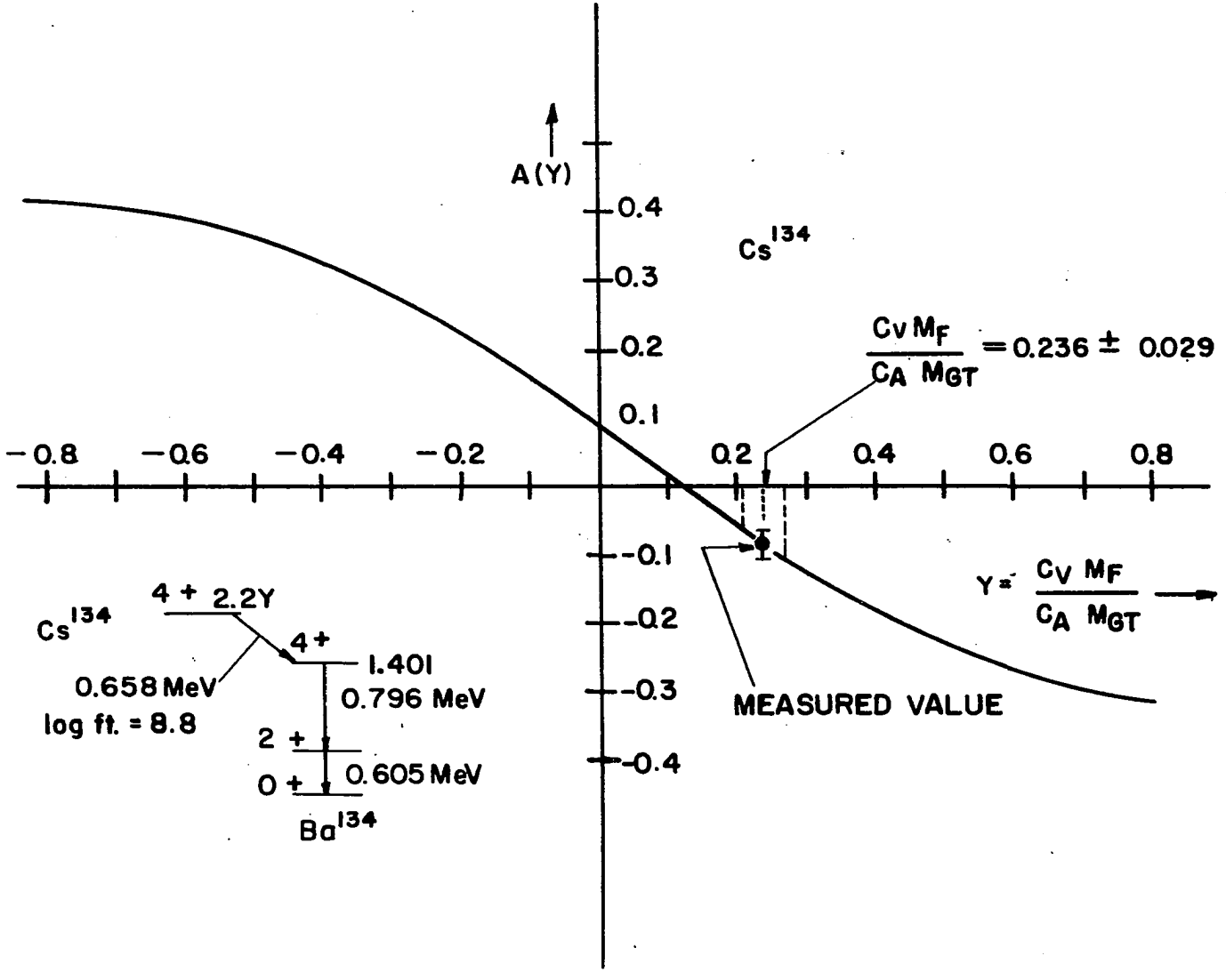
A(Y)
0.4
0.3
0.2
0.1
-0.1
-0.2
-0.3
-0.4
-0.8
-0.6
-0.4
-0.2
0.2
0.4
0.6
0.8
Cs134
Cv MF / CA MGT = 0.236 ± 0.029
Y = Cv MF / CA MGT
MEASURED VALUE
Cs134
4 + 2.2Y
4+
1.401
0.658 MeV
log ft. = 8.8
0.796 MeV
2 +
0 +
0.605 MeV
Ba134

Figure 12. Experimental results for A, the asymmetry parameter, in the case of the 621-keV beta branch of Sb^{124}. The curve is the theoretical relationship between A and Y.

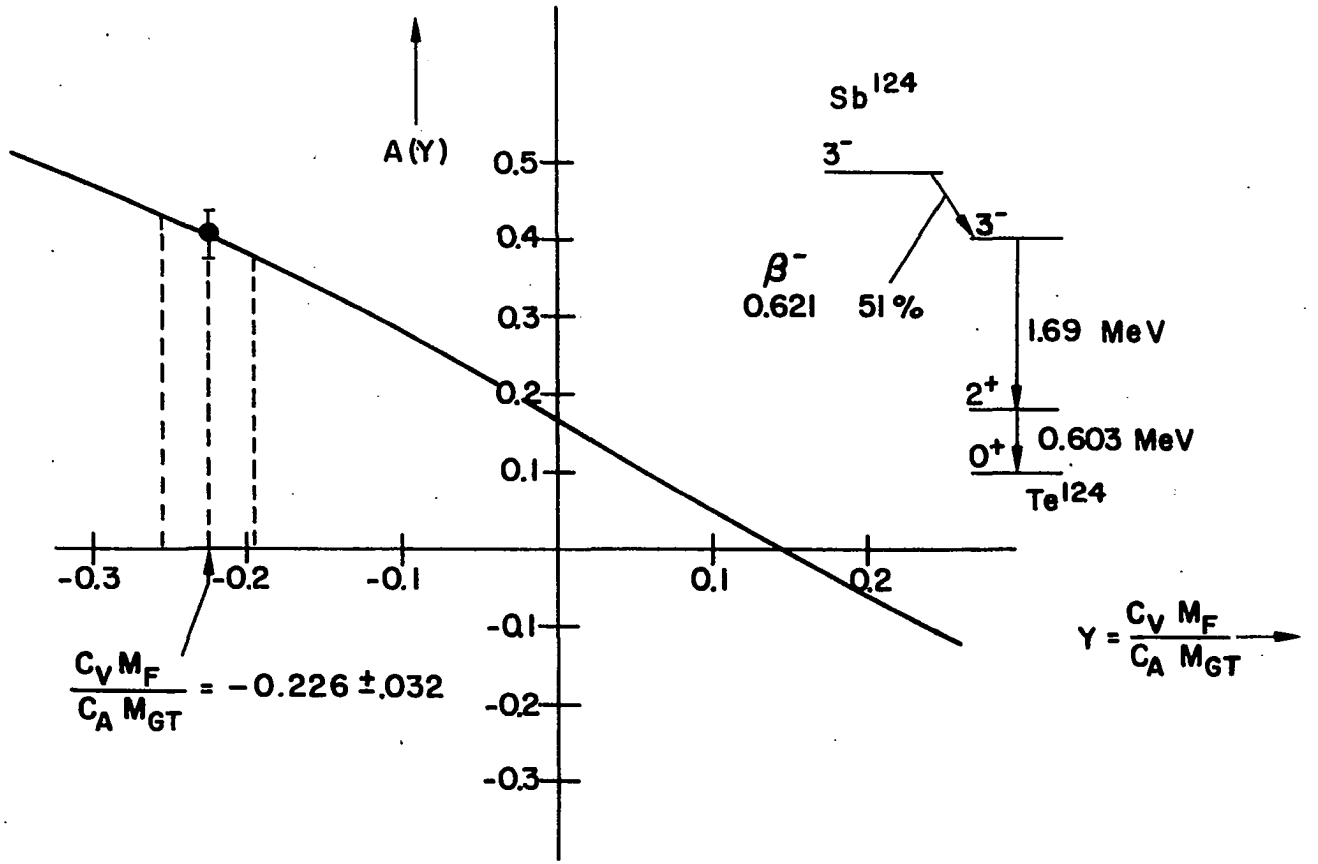
A(Y)
0.5
0.4
0.3
0.2
0.1
-0.1
-0.2
-0.3
-0.3
-0.2
-0.1
0.1
0.2
Y = $\frac{C_V M_F}{C_A M_{GT}}$
$\frac{C_V M_F}{C_A M_{GT}}$ = −0.226 ±.032
Sb^{124}
3$^-$
3$^-$
β^-
0.621
51 %
1.69 MeV
2$^+$
0.603 MeV
0$^+$
Te^{124}

C. Discussion

1. Comparison with other results

The results of various asymmetry parameter measurements in allowed transitions of Cs^{134} and Sb^{124} are shown in Table 5.

Table 5. Comparison of experimental values of the asymmetry parameter A

Nuclide	Reference		A
Cs^{134}	Mann et al.	(44)	-0.074 ± 0.022
	Daniel et al.	(60)	-0.13 ± 0.02
	Present Work		-0.088 ± 0.019
Sb^{124}	Mann et al.	(69)	+0.208 ± 0.015
	Present Work		+0.407 ± 0.030

The value measured in this investigation for Cs^{134} in an agreement with that obtained by Mann et al., but disagrees with the value reported by Daniel and co-workers. It should be noted, however, that the disagreement with the latter is not as serious as that which exists between many other measurements (see Section C, Chapter I).

It is possible that some of the difference may be due to a lower beta discriminator level used by Daniel et al. Their reported value was an average of two runs with beta discriminator levels at 95 keV and 150 keV. Such settings would include a larger percentage of the second-forbidden 410-keV branch along with the 658-keV beta branch of principal

interest. The value reported in the present work was the average of -0.095 ± 0.024 and -0.081 ± 0.024 obtained for two different sources with beta discriminator settings at 256 keV and 296 keV. The lower result was obtained for the higher discriminator setting. Using what was apparently an even higher beta energy discriminator level, Mann et al. obtained the lowest value of A. Because of its small branching ratio, variously reported to be between 2 and 9% (23,83), the contribution of the 410-keV beta branch to the coincidence counting rate would not be expected to be very significant. Therefore it is doubtful that the existing disagreement could be due entirely to different beta discriminator settings. However it is difficult to estimate the effect that even a small contribution of the second-forbidden 410-keV branch would have on the measured asymmetry.

The reason for the disagreement between the Sb^{124} results is not clear. Some differences in experimental technique were noted however. The value obtained in the present work was an average of three measurements with different sources (80-90 μC) at rather low coincidence counting rates. Each source was run for a period of about 10 days, and results of three measurements agreed to within statistical error. Mann et al. measured the asymmetry parameter using a 300 μC source at high counting rates for about 4 days. (Mann, L. G., Chemistry Division, Lawrence Radiation Lab., Livermore, California. Sb^{124} beta-gamma circular polarization measurements. Private communication. 1964).

Scattering in the source material for a 300 μC source would be expected to be more severe than in the case of the sources used in the present work. Coincidences from backscattered beta rays would tend to reduce the observed asymmetry. However, the contribution to the coincidence

counting rate from backscattered beta rays is thought to be small.

The Livermore group used a beta pulse height selector which initially accepted all beta rays above 207 keV but, because of photomultiplier fatigue under the high counting rates used, drift was observed for about 12 hours before stability was reached. However, no significant change was observed in the asymmetry during the period required for stabilization. By using a 70 cps magnet the Livermore group could tolerate a severe gain shift provided they could obtain a reasonable average for v/c under these changing conditions. The effects of higher energy beta rays on the coincidence asymmetry were determined in a second experiment with the beta discriminator set at 615 keV. This yielded a value of A = -0.136 with a large statistical error. Their measured asymmetry parameter corrected for the effect of higher energy betas was estimated by Mann to be no greater than 0.266 (although the value 0.208 was quoted in their final results).

In contrast the antimony data in the present work was obtained with a beta discriminator window. The lower (upper) discriminator was set at approximately 140 keV (490 keV). Thus there was no contribution from higher energy betas. In addition, phototube fatigue was not severe at the counting rates used so that spectral drift in the beta pulse height window was not significant.

In the present work a 4" I.D. magnet with a 5" lead absorber and an average scattering angle of 56° was used. The Livermore group used forward Compton scattering from a 4.75" I.D. magnet with a 4" Hevimet central absorber and an average scattering angle of 53°. The calculated relative detection efficiencies were similar being 0.958 (this work) and approxi-

mately 0.89 (Livermore). (Note that a smaller value of the relative detection efficiency would be expected for an analyzer with a smaller average scattering angle). The gamma-ray absorber penetration effect should be similar for the two geometries, but apparently little penetration was noted by the Livermore group. In contrast, a value of f_{np} = 31% was obtained in the present work for the fraction of coincidences resulting from Sb^{124} gamma rays scattered from nonpolarized material. Under the assumption that the penetration effect cancels in the relative comparison of Sb^{124} with Co^{60} and assuming the relative polarization detection efficiency 0.89 calculated by the Livermore group, the asymmetry parameter of 0.407 obtained in this investigation would be reduced to 0.33. Such a result is still considerably higher than that of Livermore. Consequently the disagreement cannot be explained by the effects discussed above.

Another difference in experimental technique was noted in energy selection of scattered gamma rays. The Livermore group used a discriminator which accepted all scattered gamma rays above approximately 660 keV. In the present work a gamma window was used (see Figure 7) which selected gamma rays between 515 keV and 1 MeV. Such a window was chosen to obtain a large coincidence counting rate without detecting scattered gamma rays from the strong 603-keV transition. Moreover, a contribution from high energy gamma rays penetrating the central absorber was excluded. With regard to the contamination from other gamma rays accepted by such a window, it was estimated that 89% of the coincidence counting rate was due to the principal gamma ray of interest. Moreover, the effect of the contaminants due to allowed transitions on the asymmetry parameter was not significant. Only 4% of the coincidence counting rate was due to gamma rays whose

effect on the asymmetry parameter could not be taken into account.

In view of the difference in results which could not be explained clearly by the differences in technique discussed above, more measurements are recommended.

2. Spin assignment for Cs^{134}

Though indirect evidence tends to support the 4^+ spin assignment to the 1.401 MeV level in Ba^{134}, a 3^+ assignment has also been suggested (83). Under a 3^+ assumption the Fermi to Gamow-Teller matrix element ratio vanishes for the 658-keV beta transition of cesium. The measured parameter A is then just a function (39) of the gamma-ray multipole mixing ratio Δ of 2^{L+1} - pole to 2^L - pole radiation. A comparison of the measured value $A = -0.088 \pm 0.019$ with the computed theoretical curve $A(\Delta)$ indicated disagreement with the 3^+ assignment for $\Delta < 0.8$ but reasonable agreement for $0.9 < \Delta < 2.0$. Since appreciable E2/M1 mixing might occur in the 700 keV gamma ray from the 1.401 MeV level, the 3^+ assignment cannot be entirely ruled out by these measurements as was inferred by Mann et al. (44) from their measured value $A = -0.074 \pm 0.022$ and the assumption of dipole radiation only.

Spin assignments for the principal levels in Sb^{124} are firmly established and will not be discussed here.

3. Fermi matrix elements and isospin impurities

From the ft value for the beta transition and the experimentally determined matrix element ratio, the Fermi matrix element was calculated for each nuclide of interest (using Equation 4). The results are shown in Table 6.

Table 6. Fermi matrix elements and impurity coefficients calculated from the results of this investigation

Nuclide	Log ft	Y	M_F	Isospin		Impurity Admixture
				Parent	Daughter	
Cs^{134}	8.8	0.236	-7.27×10^{-4}	12	11	-1.5×10^{-4}
Sb^{124}	7.7	-0.226	2.47×10^{-3}	11	10	5.3×10^{-4}

Although the ratios Y for cesium and antimony represent some of the largest measured (29), the Fermi matrix elements were found to be very small. This is an indication in each case of a relatively small Gamow-Teller component rather than a serious violation of the isotopic spin selection rule (rigorous adherance to the rule would require that $M_F = 0$).

Blin-Stoyle and Novakovic (16) have calculated theoretical expressions for Fermi matrix elements in a few decays characterized by $\Delta T = \pm 1$. The Fermi matrix element was given by them in the form

$$M_F = \alpha \left[(T - T_Z)(T + T_Z + 1)\right]^{\frac{1}{2}} , \qquad (19)$$

where T is the isospin quantum number. The parameter α is a measure of the isospin impurity due to charge dependent effects and, if the CVC theory does not hold, due additionally to meson exchange effects in the nucleus. The values of α shown in Table 6 were calculated for cesium and antimony from Equation 19 assuming $T_Z = T - 1$. To first order the isobaric impurities responsible for a non-vanishing Fermi matrix element are those of the daughter nucleus for β^- decays (16). The magnitude of α in

either case indicated only small admixture into the daughter state by the analog state of the parent.

The important information derived from this experimental investigation has thus been the absolute values and the relative phases of the Fermi matrix element and Gamow-Teller matrix element for allowed beta transitions of Cs^{134} and Sb^{124}. There is a need for theoretical calculations of the Fermi matrix elements which apparently have not yet been attempted for these nuclides. In view of the small magnitudes of M_F determined above and the theoretical calculations for other cases (16), it was thought difficult to separate meson exchange effects from charge dependent effects for these nuclides and thus test the CVC theory. However information might be gained concerning charge dependent effects in the beta transitions of these medium weight nuclei in comparing these experimental results with calculations performed under the assumptions of the CVC theory.

The relative phases of the matrix elements have been found to be negative for Cs^{134} and positive for the allowed transition in Sb^{124}. This raises the question as to the significance of the phases of the matrix elements in these and other allowed transitions for which experimental information is now available.

4. Recommendations

Several technical improvements could be made to obtain more precise results. Modifying the electronics to accept extremely high counting rates would be very desirable. This would require gain stabilization of the photomultiplier tubes (which is quite difficult for spectra with no sharp peaks). A longer central absorber with a Hevimet core would be

recommended. Use of a solid state detector for beta rays should be considered. A magnet capable of rapid alternation such as that being used at Livermore (84) would certainly improve stability.

With the above technical improvements, certain allowed transitions in Eu^{152} could be investigated, for example. Other cases of even greater importance include Eu^{152m} (verification of spin assignment of the ground state) and Hf^{181} (possible depolarization of nuclei in a long lived excited state). Also, there has been some disagreement in results for Sc^{44} (29). In addition considerable work remains in allowed transitions of short lived isotopes.

The work could be extended to forbidden transitions. The interpretation of the results of measurements of circular polarization in forbidden beta transitions is complicated by the fact that the number of nuclear matrix elements that affect even a first-forbidden transition is much larger than for allowed transitions. Several first-forbidden cases have yet to be examined (23,29), but the extension of measurements to more highly forbidden beta transitions awaits further theoretical developments.

Finally, it would be worth while to thoroughly investigate the dependence of the circular polarization on v/c for Mn^{56} and Co^{60}. The issue which has not yet been settled and which is important to the theory of parity nonconservation is whether the v/c law is followed exactly or whether small deviations exist.

V. SUMMARY

In this investigation measurements were made of the circular polarization of gamma rays following the beta decay of Cs^{134} and Sb^{124}. The method involved selecting beta-gamma coincidences with a fixed angle θ between the directions of emission of the gamma ray and the beta particle, and simultaneously detecting the circular polarization of the gamma ray. The degree of circular polarization was measured using forward Compton scattering of the photons from partially-polarized electrons available in magnetized iron. From the observed relative coincidence counting rate for opposite orientations of the polarization analyzer magnet the circular polarization asymmetry parameter A was determined.

The value obtained for the asymmetry parameter for Cs^{134} was found in this investigation to be -0.088 ± 0.019. From the theoretical relation (computed assuming the (V-A) beta interaction) between the asymmetry parameter and the Fermi to Gamow-Teller matrix element ratio

$$Y = \frac{C_V M_F}{C_A M_{GT}} ,$$

the corresponding matrix element ratio for the Cs^{134} allowed beta transition was determined to be $Y = 0.236 \pm 0.029$. The asymmetry parameter measured for the allowed 0.621-MeV beta transition of Sb^{124} was $A = +0.407 \pm 0.030$. The corresponding Fermi to Gamow-Teller matrix element ratio for this transition was found to be $Y = -0.226 \pm 0.032$.

VI. LITERATURE CITED

1. Lee, T. D. and C. N. Yang, The Physical Review, 104, 254 (1956).
2. Wu, C. S., E. Ambler, R. W. Hayward, D. D. Hoppes, and R. P. Hudson, The Physical Review, 105, 1413 (1957).
3. Wu, C. S., Reviews of Modern Physics, 31, 783 (1959).
4. Alder, K., B. Stech, and A. Winther, The Physical Review, 107, 728 (1957).
5. Morita, M. and R. S. Morita, The Physical Review, 107, 1316 (1957).
6. Blatt, J. M. and V. F. Weisskopf, Theoretical Nuclear Physics, John Wiley and Sons, Inc., New York. 1952.
7. Konopinski, E. J., Reviews of Modern Physics, 15, 209 (1943).
8. Skyrme, T., Progress in Nuclear Physics, 1, 115 (1950).
9. Weidenmüller, H. A., Reviews of Moderns Physics, 33, 574 (1961).
10. Rose, M. E. Analysis of Beta-Decay Data. In Ajzenberg-Selove, ed., Nuclear Spectroscopy, Part B, pp. 811-833, Academic Press, Inc., New York. 1960.
11. Rose, M. E., N. M. Dismuke, C. L. Perry, and P. R. Bell. Tables of Fermi functions. In Siegbahn, K., ed., Beta-and Gamma-Ray Spectroscopy, pp. 875-883, Interscience Publishers, Inc., New York. 1955.
12. Sherr, R. and R. H. Miller, The Physical Review, 93, 1076 (1954).
13. Gerhart, J. B., The Physical Review, 109, 897 (1958).
14. Pohm, A. V., R. C. Waddell, and E. N. Jensen, The Physical Review, 101, 1315 (1956).
15. Porter, F. T., F. Wagner, Jr., and M. S. Freedman, The Physical Review, 107, 135 (1957).
16. Blin-Stoyle, R. J., and L. Novakovic, Nuclear Physics, 51, 133 (1964).
17. Blin-Stoyle, R. J., Rutherford International Conference Proceedings, 1961, 677 (1961).
18. Bardin, R. K., C. A. Barnes, W. A. Fowler, and P. A. Seeger, Physical Review Letters, 5, 323 (1960).

19. Salam, A., Nuovo Cimento, 5, 299 (1957).

20. Landau, L., Nuclear Physics, 3, 127 (1957).

21. Lee, T. D. and C. N. Yang, The Physical Review, 105, 1671 (1957).

22. Konopinski, E. and H. M. Mahmoud, The Physical Revew, 92, 1045 (1953).

23. Nuclear Data Sheets, National Academy of Sciences - National Research Council, Washington, D. C.

24. Herrmannsfeldt, W. B., D. R. Maxson, P. Stähelin, and J. S. Allen, The Physical Review, 107, 641 (1957).

25. Hermannsfeldt, W. B., R. L. Burman, P. Stähelin, J. S. Allen, and T. H. Braid, Physical Review Letters, 1, 61 (1958).

26. Goldhaber, M., L. Grodzins, and A. W. Sunyar, The Physical Review, 109, 1015 (1958).

27. Nordberg, M. E., F. B. Morinigo, and C. A. Barnes, The Physical Review, 125, 321 (1962).

28. Burgy, M. T., V. E. Krohn, T. B. Novey, G. R. Ringo, and V. L. Telegdi, The Physical Review, 120, 1829 (1960).

29. Estulin, I. V. and A. A. Petushkov, Soviet Physics - Uspekhi, 7, 101 (1964).

30. Kofoed-Hansen, O. and C. J. Christensen, Encyclopedia of Physics (Handbuch der Physik), 41, No. 2, 1 (1962).

31. Sudarshan, E. C. G. and R. E. Marshak, The Physical Review, 109, 1860 (1958).

32. Sakurai, J. J., Nuovo Cimento, 7, 649 (1958).

33. Feynman, R. P. and M. Gell-Mann, The Physical Review, 109, 193 (1958).

34. Freeman, J. M., J. H. Montague, G. Murray, R. E. White, and W. E. Burcham, Physics Letters, 8, 115 (1964).

35. Wu, C. S., Reviews of Modern Physics, 36, 618 (1964).

36. Blin-Stoyle, R. J., Nuclear Physics, 57, 232 (1964).

37. Wheatley, J. C., W. J. Huiskamp, A. N. Diddens, M. J. Steenland, and H. A. Tolhoek, Physica, 21, 841 (1955).

38. Schopper, H., The Philosophical Magazine, 2, 710 (1957).

39. Morita, M., The Physical Review, 107, 1729 (1957).

40. Gaponov, Y. V. and V. S. Popov, Nuclear Physics, 4, 453 (1957).

41. Steffen, R. M., The Physical Review, 115, 980 (1959).

42. Appel, H., Zeitschrift für Physik, 155, 580 (1959).

43. Appel, H., H. Schopper, and S. D. Bloom, The Physical Review, 109, 2211 (1958).

44. Mann, L. G., S. D. Bloom, and R. J. Nagle, The Physical Review, 127, 2134 (1962).

45. Mann, L. G., S. D. Bloom, and R. J. Nagle, Nuclear Physics, 30, 636 (1962).

46. Freiberg, E. and V. Soergel, Zeitschrift für Physik, 162, 229 (1961).

47. Castle, R. T. and R. W. Finley, The Physical Review, 134B, 929 (1964).

48. Bloom, S. D., L. G. Mann, and J. A. Miskel, The Physical Review, 125, 2021 (1962).

49. Forster, H. H. and N. L. Sanders, Nuclear Physics, 15, 683 (1960).

50. Boehm, F. and A. H. Wapstra, The Physical Review, 109, 456 (1958).

51. Daniel, H. and M. Kuntze, Zeitschrift für Physik, 162, 229 (1961).

52. Daniel, H., D. Mehling, O. Muller, P. Schmidlin, H. Schmitt, K. S. Subudhi, and E. Neuberger, Nuclear Physics, 45, 529 (1963).

53. Boehm, F., The Physical Review, 109, 1018 (1958).

54. Bloom, S. D., L. G. Mann, and J. A. Miskel, Physical Review Letters, 5, 326 (1960).

55. Mayer-Kuckuk, T., R. Nierhaus, and U. Schmidt-Rohr, Zeitschrift für Physik, 157, 586 (1960).

56. Boehm, F. and J. Rogers, Nuclear Physics, 33, 118 (1962).

57. Lundby, A., A. P. Patro, and J. P. Stroot, Nuovo Cimento, 7, 891 (1957).

58. Jungst, W. and H. Schopper, Zeitschrift für Naturforschung, 13A, 505 (1958).

59. Singru, R. M. and R. M. Steffen, Nuclear Physics, 43, 537 (1963).

60. Daniel, V. H., J. Hüfner, and O. Mehling, Annalen der Physik, 12, 106 (1963).

61. Miskel, J. A., L. G. Mann, and S. D. Bloom, The Physical Review, 132, 1130 (1963).

62. Daniel, H., O. Mehling, O. Müller, and K. S. Subudhi, The Physical Review, 128, 261 (1962).

63. Haase, E. L., H. A. Hill, and D. B. Knudsen, Physics Letters, 4, 338 (1963).

64. Bloom, S. D., L. G. Mann, R. Polichar, J. R. Richardson, and A. Scott, U. S. Atomic Energy Commission Report, UCRL-7230 [California University, Berkeley, Radiation Laboratory] (1963).

65. Bouchiat, C. C., Physical Review Letters, 3, 516 (1959).

66. Lobashov, V. M. and V. A. Nazarenko, Soviet Physics JETP, 15, 257 (1962).

67. Kotani, T., The Physical Review, 114, 795 (1958).

68. Steffen, R. M., The Physical Review, 123, 1787 (1961).

69. Mann, L. G., D. C. Camp, J. A. Miskel, and R. J. Nagle, Bulletin of the American Physical Society, Ser. 2, 9, 395 (1964).

70. Schopper, H., Nuclear Instruments, 3, 158 (1958).

71. Steffen, R. M., The Physical Review, 118, 763 (1960).

72. Whetstone, A. and S. Kounosu, The Reviews of Scientific Instruments, 33, 423 (1962).

73. Zumwalt, L. R., U. S. Atomic Energy Commission Report, AECU-567 [Technical Information Division, Oak Ridge National Laboratory, Oak Ridge, Tenn.] (1950).

74. Nelms, A. T. Energy Loss and Range of Electrons and Positrons. National Bureau of Standards Circular, 577, Supplement, 1 (1950).

75. Lipps, F. W. and H. A. Tolhoek, Physica, 20, 395 (1954).

76. Grodzins, L., Progress in Nuclear Physics, 7, 163 (1959).

77. Davisson, C. M. and R. D. Evans, Reviews of Modern Physics, 24, 79 (1952).

78. Vegors, Jr., S. H., L. L. Marsden, and R. L. Heath, U. S. Atomic Energy Commission Report, IDO-16370 [Idaho Operations Office, A. E. C.] (1958).

79. Huber, H., S. Galster, and H. Schopper, Nuclear Instruments and Methods, 21, 338 (1963).

80. Beers, Y. Introduction to the Theory of Error, Addison-Wesley Publishing Co., Inc., Reading, Mass. 1956.

81. Alexander, P. and R. M. Steffen, The Physical Review, 124, 150 (1961).

82. Kotani, T. and M. Ross, The Physical Review, 113, 622 (1959).

83. Trehan, P. N., J. D. French, and M. Goodrich, The Physical Review, 131, 2625 (1963).

84. Pechacek, R. E., L. G. Mann, S. D. Bloom, and R. M. Rodriques, The Reviews of Scientific Instruments, 35, 58 (1964).

VII. ACKNOWLEDGMENTS

The author wishes to thank Dr. D. J. Zaffarano for his valuable suggestions and support.

Grateful acknowledgment is also given to the following people for their assistance during this investigation:

Mr. R. H. Brown and members of the Instrument Shop, who did the machine work on the apparatus.

Mr. E. E. Sobottka, who prepared the sources.

Mr. J. W. Case, who assisted in constructing the equipment.

Mr. W. A. Rhinehart who designed the automatic control system.

Members of the Instrumentation Group, who kept the electronic circuitry in good operating condition, and

Mr. R. W. Carr, whose assistance in taking and analyzing the data as well as preparing the source holders was invaluable.

Above all the author wishes to express his deepest thanks to Dr. W. L. Talbert for continuing support, suggestions, and encouragement both as adviser and friend.